STRESS ANALYSIS AND FATIGUE LIFE PREDICTION OF PSEUDOELASTIC NITI SHAPE MEMORY ALLOY TAPERED STRESS JOINT VIA FINITE ELEMENT METHOD

A Thesis

by

A-LIM KIM

Submitted to the Office of Graduate and Professional Studies of
Texas A&M University
in partial fulfillment of the requirements for the degree of

MASTER OF SCIENCE

Chair of Committee,	James Boyd
Committee Members,	Darren Hartl
	Moo-Hyun Kim
Intercollegiate Faculty Chair,	Efstratios Pistikopoulos

August 2017

Major Subject: Energy

ABSTRACT

This research concerns Tapered Stress Joints (TSJ), which connect the offshore platform and the top tensioned riser transporting the produced oil. In this paper, the TSJ applying the pseudoelastic effect of Shape Memory Alloys (SMAs) is proposed to reduce the stress concentration at the hang-off point, thereby increase the fatigue life of the TSJ and allowing the TSJ to survive extremely large rotations due to storms, explosions, and collisions. To this end, the finite element analysis (FEA) of the pseudoelastic NiTi TSJ system is implemented using the Abaqus/Standard program and with a user subroutine (UMAT). The FEA assumes the applied top tension at the top of the TSJ and the cyclic rotation to the right and left. By using the result of the FEA, the stress analysis and the fatigue life prediction is implemented.

In the stress analysis, whether the pseudoelastic NiTi TSJ satisfies the design criteria based on the API Standard 2RD was examined. The elastic and pseudoelastic behavior of the NiTi TSJ was also analyzed by comparison to the steel and the titanium TSJ. The plastic yield angle and the maximum allowable angle of rotation for the operating temperature are obtained. The stress data in a cyclic rotation is used for the fatigue life prediction, which is based on the SWT and Morrow equation.

In conclusion, it is demonstrated that the pseudoelastic SMA TSJ shows the better performance than the steel and titanium TSJ regarding the stress and the fatigue life. Particularly, the conclusion of this thesis suggests that martensite transformation of

the NiTi TSJ is useful to reduce the stress, improve structural integrity, and extend the service life.

DEDICATION

To my father Kwang-Hun, mother Hye-Kyung, and my beloved sister Ye-Lim

ACKNOWLEDGEMENTS

I would like to thank my committee chair, Prof. Boyd, and my committee members, Prof. Hartl, and Prof. Kim for their guidance and support throughout the course of this research. Especially Prof. Boyd advised my work with great patience.

Thanks also go to my friends and colleagues, John and Alex for advising my job and I learned a lot from these two promising researchers.

Finally, thanks to my mother, father, and my sister for their encouragement, patience, and love.

CONTRIBUTORS AND FUNDING SOURCES

Contributors

This work was supervised by a thesis committee consisting of Professor James Boyd and Professor Darren Hartl of the Department of Aerospace Engineering and Professor Moo-Hyun Kim of the Department of Ocean Engineering.

Portions of this research were conducted with the advanced computing resources provided by Texas A&M High Performance Research Computing.

All work conducted for the thesis was completed by the student, under the advisement of Professor James Boyd, Research Associate John Rohmer, and Post-Doctoral Research Associate Alexandros Solomou of the Department of Aerospace Engineering.

Funding Sources

Graduate study was supported by a fellowship from Engineering Development Research Center (EDCR), Seoul National University, South Korea.

TABLE OF CONTENTS

Page

LIST OF FIGURES

Page

LIST OF TABLES

Page

1. INTRODUCTION

1.1 Motivation

The offshore platform is a facility that produces crude oil in a subsea reservoir thousands of feet below, experiencing sea waves and wind in the middle of the sea. Fixed type platform was used at shallow water depth in the past, but floating type platform is commonly used and getting bigger due to deeper water depth and climate change as production takes place farther on the land. Floating production at deep-water depths has increased the capacity of the platform further, and the structure is influenced more from the marine environment and the weather environment. The related risks have increased due to changes in the operating environment of these floating platforms.

The lesson learned from the accident like Macondo disaster at the Gulf of Mexico is that perhaps minor flaws in the offshore platform can lead to catastrophic accidents and that these incidents are too painful to return to its original state. Various technologies and standards have been developed to prevent such accidents and to ensure the safety and reliability of offshore platform operation. One of the goals of these attempts is to increase structural integrity through the application of stronger materials.

There are primarily two critical points regarding the safe and reliable transportation of the produced fluid: touch-down zone (TDZ) and hang-off point. Significantly, high-stress concentration occurs at these points, so strength and fatigue issue has been intensively researched. Regarding the material application to these points, the high-strength steel, the titanium alloys or various kinds of alloys have been

suggested to increase the strength of the structure. Additionally, many researchers have developed the structures or components to reduce the concentrated stress at these critical points. For example, the tapered stress joint (TSJ) reduces the bending stress at the hang-off point by its tapered section connecting the platform and the production riser. Moreover, applying the titanium that has higher yield stress and lower elastic modulus than steel to the TSJ contributes to reducing the stress concentration significantly.

1.2 Overview of Offshore Floating Production Systems

1.2.1 Floating Production Platforms

Offshore production at greater depths exceeding 1,500 ft required different platforms types with different features. The type of floating platform developed for the corresponding water depth is shown in Table 1 (API, 2017). These various platforms remain highly effective technologically and are used worldwide in offshore production.

Table 1 Types of Floating Platforms (API, 2017)

Water Depth	Platform Type
1,500 – 3,000 ft	Compliant towers
3,000 – 5,000 or 7,000 ft	Tension leg platforms (TLP)
5,000 – 7,000 ft	Floating production systems (FPS), Floating Production, Storage & Offloading System (FPSO)
3,000 – 7,500 ft	Spar platform

Compliant towers are steel truss structures that utilize less seabed footprint compared to the conventional fixed steel-jacket structure as shown in Figure 1. Although

the compliant towers resemble the fixed jacket platform at a quick glance, they yield to both wind and wave dynamics similarly as floaters.

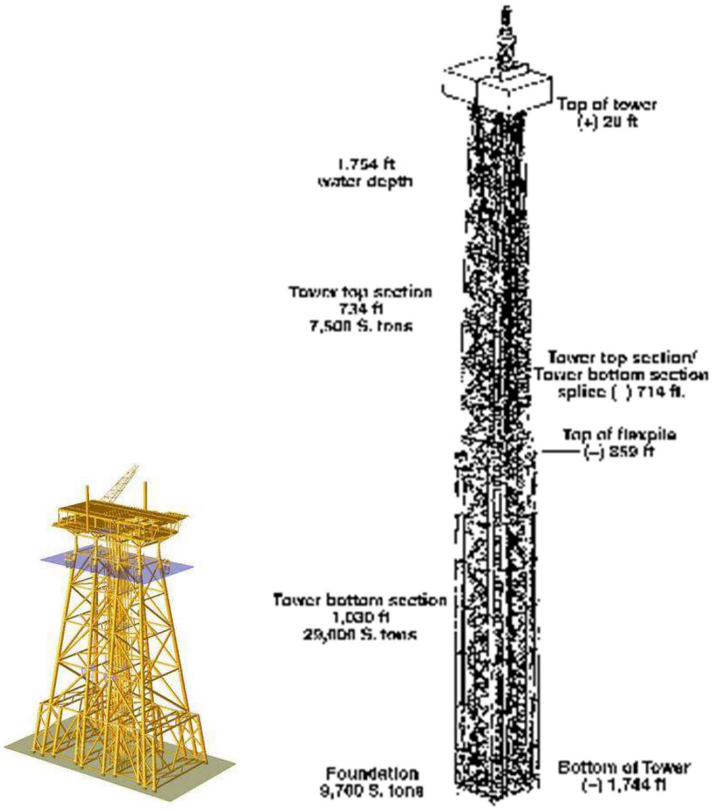

Figure 1 Fixed Jacket Platform (Left) Reprinted from (offshorellc, 2017) and Compliant Tower (Right) Reprinted from (Furlow, 2017)

Tension leg platforms (TLP) are floating platforms that mainly operate at water depths of 3,000 ft to 7,000 ft. The TLP is tethered to the seabed and maintained in a horizontal state by a number of tendons, which are kept in tension to suppress the heave

motions as shown in Figure 2. The TLP is largely distinguished from a semisubmersible in the fact that the buoyancy requirement for a TLP is usually two to five times greater than that of a semisubmersible.

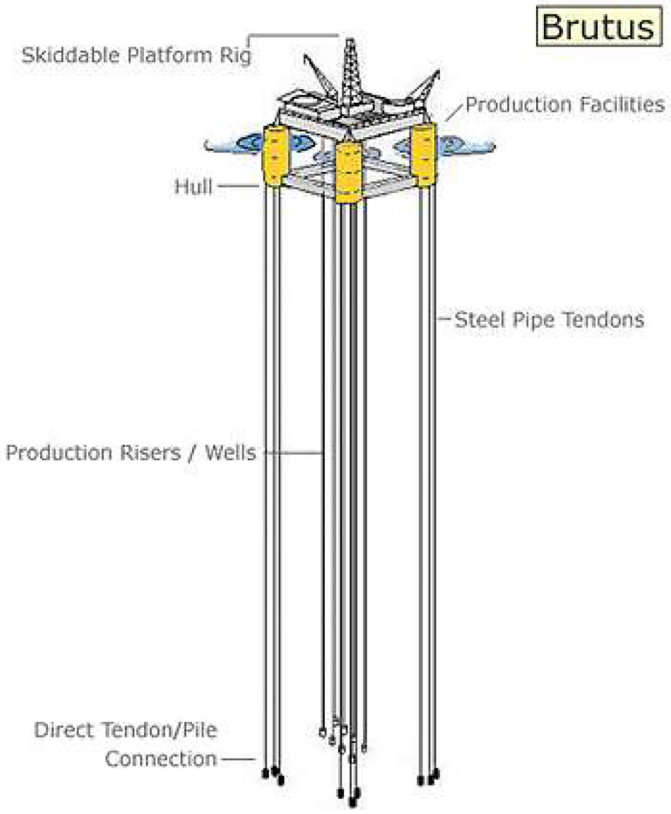

Figure 2 Tension Leg Platform (TLP) Reprinted from (offshore-technology, 2017)

Floating production systems (FPS) and Floating Production, Storage & Offloading System (FPSO) are usually operated in water depth up to 7,000 ft. FPS consists of a semisubmersible that is dynamically positioned by rotating thrusters or

anchored in place with wire rope and chain and FPSO consists of a large tanker type vessel moored to the seabed as shown in Figure 3. In a similar water depth, the Spar platform type is also commonly used and Spar is moored with wires anchored to the seabed as shown in Figure 3.

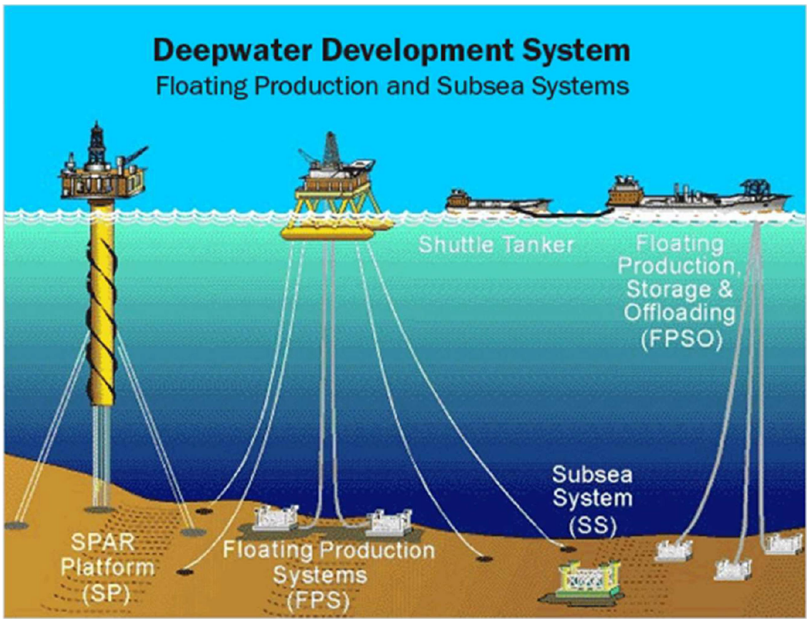

Figure 3 Floating Production System (FPS), Floating Production, Storage & Offloading System (FPSO) and Spar Platform Reprinted from (API, 2017)

1.2.2 Riser System

A riser system mainly consists the riser and the integrated riser components. A riser is a pipe or the conduit for transporting the produced fluid flow from the reservoir to the floating platform. There are many types of risers, including drilling risers,

completion risers, export risers, injection risers, and production risers. The main function of risers is to transport fluids and gas from a seabed to a floating platform, as well as transport various well operation tools and options. This thesis will focus on the production risers which transport fluids from the reservoir. Production risers are typically operated from a floating platform and absorb the motion of the platform. Therefore, which type of the production risers will be used should be carefully determined considering the platform type. There are mainly two types of the production risers; top tensioned riser and compliant riser.

The top tensioned riser is vertically installed and used with a small heave motion platform (e.g. TLP, Spar platforms, and semisubmersible). The top tensioned riser is supported by a top tension, which is applied intentionally to maintain a vertical configuration while preventing the riser from a compression or a buckling. Top tensioned risers operated from TLP's and semi-submersibles are equipped with a separate hydraulic heave compensation system to account for the floater motions and at the same time maintain a constant target value for the applied top tension (DNV, 2010). Top tension risers operated from Spar platforms are also equipped with buoyancy modules attached along the upper part of the riser to obtain the top tension.

The compliant riser is designed to absorb floater motion by changing its geometry without heave compensation systems. The most common and the simplest type of this compliant riser is a steel catenary riser (SCR) that also can be used in deep water. Compliant riser system experience significantly much larger static and dynamic

excursions when compared to top tensioned riser. Moreover, its configuration should be more carefully determined than top tensioned riser due to its geometry nonlinearity.

Production riser is terminated by a riser component which connects the riser and the platform and reduces the bending stress at the top of the riser. A pronounced peak in the bending moment distribution is normally found at the top location of the riser, which is normally denoted as a Hang-Off point. Riser joints (e.g. tapered stress joint, flex joint, or ball joint) allow for reducing this large bending stress at the Hang-Off point and transporting the fluid from the production riser into the platform. To avoid an excessive local buckling or other non-linear instabilities that are likely to result in the failure of the riser joints, the riser joints must have sufficient ductility or flexibility to endure large inelastic displacements due to repeated yielding and prevent the structure from fractures or failures. To this end, riser joints have been developed with various geometry or materials to achieve a high flexibility. The tapered stress joint (TSJ) is the most commonly used type of riser joint than other types. As its name implies, TSJ has tapered shape and consists of metallic components. The following section will discuss the TSJ and review the research related to it.

1.3 Literature Review of TSJ

As explained in Section 1.2, TSJ connects the production riser and the platform at the hang-off point and prevents stress concentration at that point. TSJ mainly consists of two metallic components, the main body and the bushing as shown in Figure 4. The design of TSJ usually focuses on the main body by assuming it is a pipe with a tapered cross-section in a longitudinal direction.

Figure 4 3D drawing of the TSJ. Reprinted from (RTI Energy Systems 2005)

There is no formal theory in designing TSJ, but it is focused on the strength and flexibility to endure the occurring stress and the repeated yielding induced by the motion

of the platform. The boundary conditions that are used in the design are known to vary by the standards that are recommended by the operating site of the platform or country; the standard criteria in the industry are that the maximum stress of the TSJ design should be less than the yielding stress of the material.

Previous research on the TSJ design has focused on the strength analysis of steel or titanium main body of TSJ by optimizing its geometry. Spark established two design methods in his book (Sparks, 2007); Design with constant curvature through the stress joint and the design with constant maximum bending stress. The boundary conditions used in both methods are the applied tension and the rotation of the structure. Spark's design methods apply to any types of the riser and the platform. Following this method, Zhang et al. designed TSJ with steel and performed sensitivity analysis to ensure that the designed TSJ can perform its function during its operation (Zhang et al., 2010). Gordon developed a numerical solution of TSJ, especially focusing on the top tensioned riser and the floating platform (Gordon et al., 2004). The boundary conditions are applied top tension and the rotation of the platform, assuming that the TSJ follows the rotation of the platform. As Gordon investigated, the greater the length of the outer diameter at the top of the TSJ, the smaller the stress at the hang-off point. In other words, the larger the difference between the outer diameter of the top and the bottom of the TSJ, the smaller the stress at the hang-off point. Therefore, it is important to optimize the geometry of TSJ considering the potential operating and environment conditions. To this end, Gordon investigated the stress distribution over the TSJ with various outer diameters at the top of the TSJ using the numerical solution and optimized the geometry of the TSJ

design, which balances the maximum stresses over the TSJ. This optimized geometry will be used in this thesis for the preliminary design of SMA TSJ.

The early TSJ was manufactured of the steel alloy. Now titanium alloy is sometimes used due to its lower elastic modulus but higher yield stress than the steel alloy. This thesis proposes to apply the SMA to the TSJ, focusing on the pseudoelastic effect of SMA.

Fatigue analysis of TSJ design was done by various authors. Yang and Zheng implemented the multiaxial analysis of the steel TSJ for deepwater SCR (Yang et al., 2012). Vargas et al. did the BS 7910 ECA for the titanium TSJ for use on a high motion floating platform in the Gulf of Mexico (Vargas et al., 2011). However, these works were done with only one set of boundary conditions. Moreover, among these works, no work applies various materials to one TSJ design and compares the results via computational analysis to find the best material applications. Therefore, this thesis proposes applying the SMA, the steel alloy, and the titanium alloy to the one optimized geometry of TSJ and comparing each case with via the finite element (FE) analysis. Moreover, the FE analysis will be implemented with the boundary conditions for the Gulf of Mexico considering the design condition of hurricanes. This kind of the first ever FE analysis of SMA TSJ will be implemented in this thesis.

1.4 Literature Review of Pseudoelastic Effect

1.4.1 Phase Transformation of Pseudoelasticity

There are largely two types of transformation of SMAs: forward transformation and reverse transformation. Forward transformation refers a phase change from an

austenite phase to a martensite phase, and the reverse transformation refers to the opposite phase change of the forward transformation. The pseudoelastic behavior related to the stress-induced transformation at temperatures above A_f. When the material is subjected to the loading, austenite phase develop into the detwinned martensite state, and return to austenite phase when the stress is released. An example of this transformation is shown in Figure 5.

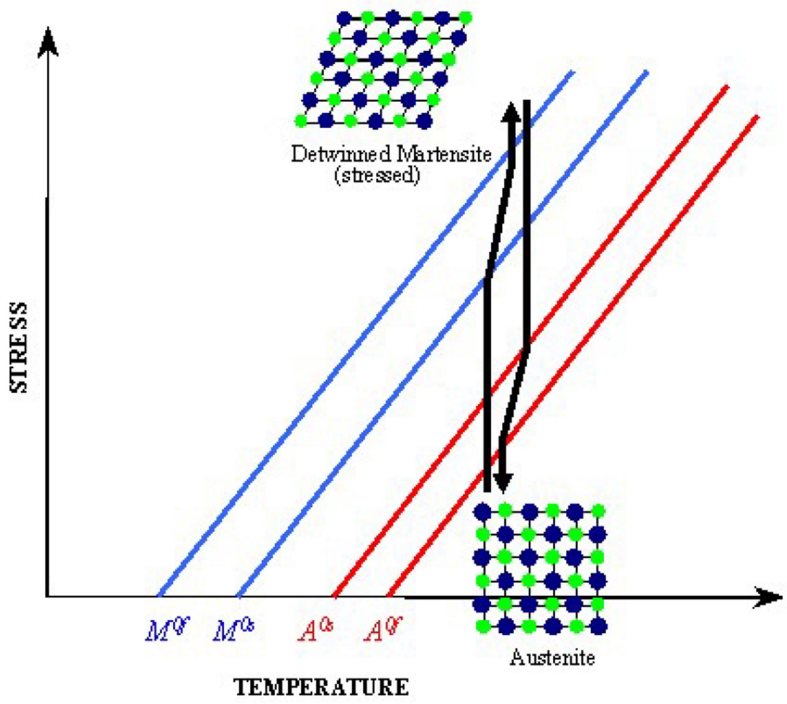

Figure 5 Pseudoelastic loading path Reprinted from (Smart Lab, 2017)

The stress-induced transformation of the pseudoelastic effect generates large inelastic strain and recovers it completely as shown in Figure 6. Ability to recover such a

large inelastic strain is the advantage of the pseudoelastic effect. The forward transformation from austenite to detwinned martensite is represented by the change in slope on the stress-strain curve. After the martensite transformation completes, the detwinned martensite is stressed with the elastic loading. When the stress is released gradually by unloading, the detwinned martensite transforms into austenite, which is accompanied by the recovery of the generated inelastic strain. This reverse transformation completes the pseudoelastic cycle resulting in a hysteresis loop as shown in Figure 6. The area of the hysteresis loop means the dissipated energy in the transformation cycle.

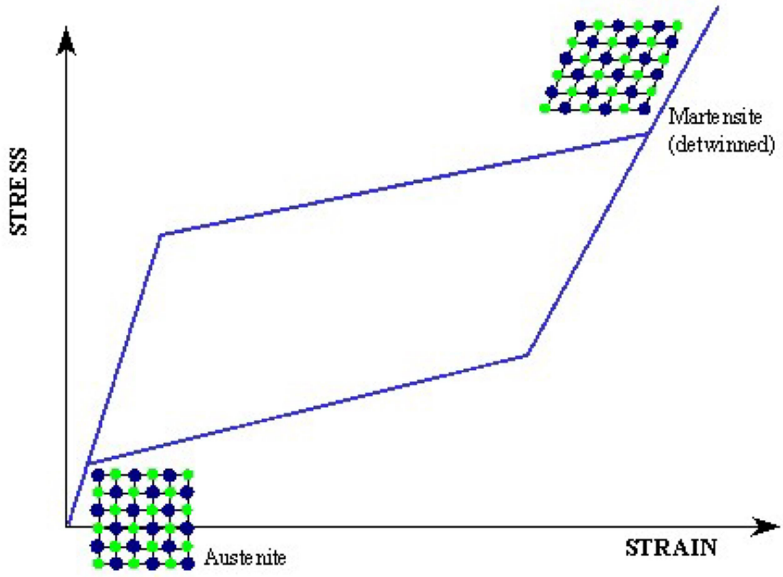

Figure 6 Pseudoelastic stress-strain diagram Reprinted from (Smart Lab, 2017)

1.4.2 Industrial Application using Pseudoelastic effect

Because of its ability to recover a large inelastic strain completely and a relatively lower stress generation, the application of pseudoelastic effect has been widely researched and implemented in a variety of industries. For example, NiTi that is a representative example of SMA can withstand much greater strains amplitudes ranging from 4% to 12% before failure than that of other metal alloys, which is around 1% or less. This section will review some application of the pseudoelastic effect cases briefly.

Pseudoelastic SMA is usually applied to the structure that is mainly subjected to the bending during its service life. It is widely applied in the biomedical industry as well as aerospace and automotive industry. The pseudoelastic effect of SMA is more commonly researched in the biomedical industry. Examples of this application include stents, filters, and orthodontic wires, etc. One notable example is an orthodontic wire. The elastic material like a stainless steel generates a large increment of stress for a small increment of increment resulting in a large force to the body. With the pseudoelastic SMA, however, there is little increase in stress with a large increase in strain. This is because of the lower elastic modulus of austenite and martensite (E_A and E_M) and the very low slope of the stress-strain curve during the transformation.

Another important advantage of the pseudoelastic SMA is that the material composition and properties can be designed for the purpose of the application. Therefore, it is possible to consider the environment of the potential application actively.

This thesis proposes to apply the pseudoelastic effect to the TSJ with a top tensioned riser to reduce the stress and increase its service life. The pseudoelastic SMA TSJ is

compared to other elastic materials (i.e. steel and titanium) regarding the stress (strength) and the fatigue life. The detailed explanations about the advantages obtained from the application of the pseudoelastic SMA than other elastic materials are as following:

- Given the same deformation of the structure, lower stress occurs in the SMA TSJ due to the lower elastic modulus and the low growth rate of the stress according to the strain during the martensite transformation.
- Due to the occurrence of the lower stress as described in 1, the fatigue life of the SMA TSJ is longer.
- Due to the lower elastic modulus, SMA TSJ has a greater flexibility than the steel or titanium TSJ.
- The yield stress of SMA is generally higher than the steel or the titanium that are used in manufacturing TSJ currently.
- SMA can recover a relatively larger inelastic strain, whereas the steel and the titanium cannot.

1.5 Outline of Thesis

This thesis serves to describe the first ever FE analysis of the application of SMA to the TSJ as described and is organized as follows:

- Chapter 2 provides an overview of various stress analysis methods. This includes an introduction of an analytical solution of TSJ design with a top tensioned riser and a description of a recommended design criteria used in the offshore industry. The overview of the constitutive models of both the elastic

materials and the SMA for the FE analysis is also discussed. Finally, the stress-life curves to predict the fatigue life are reviewed.

- Chapter 3 discusses the detailed description of the FE modeling process of SMA TSJ system, which is done using the Abaqus Finite Element Analysis (FEA) program. Types and magnitude of the loads and the boundary conditions for the analysis are also discussed, especially calculating the applied top tension. Also, the selection of transformation temperatures for the pseudoelastic effect is implemented in this chapter.
- Chapter 4 analyzes the results obtained from the FE analysis. The stress analysis and the fatigue analysis of the pseudoelastic SMA TSJ system are implemented.
- Chapter 5 summarizes the results of this thesis and makes a conclusion. The future work required for accurate analysis will also be discussed.

2. OVERVIEW OF STRESS ANALYSIS METHOD

2.1 Modeling of TSJ System

2.1.1 Mathematical Tool for Designing TSJ System

Designing the TSJ is a nonlinear problem since its cross section changes along with the length, and this is why it has a term “tapered” in its name. The purpose of the TSJ is to reduce the bending stress at the Hang-off point to avoid the stress concentration. Therefore, calculating the stress distribution is practically important in the design and the simulation stage. To this end, largely two methods of designing TSJ have been developed so far. These two methods assume different compositions of system and boundary conditions. One method developed by Spark has two different assumptions for each analytical solution, and both methods apply to the TSJ with any risers (Sparks, 2007). However, those methods are more suitable to the preliminary design of TSJ, since it cannot produce exact stress distribution due to the limited assumptions. The other method developed by Gordon can be applied only to the TSJ model with a top tensioned riser (Gordon et al., 2004); however, it can produce a numerical solution of the model by solving the nonlinear differential equation. In this thesis, Gordon’s numerical solution is briefly introduced. The geometry for the TSJ and the top-tensioned riser is shown in Figure 7.

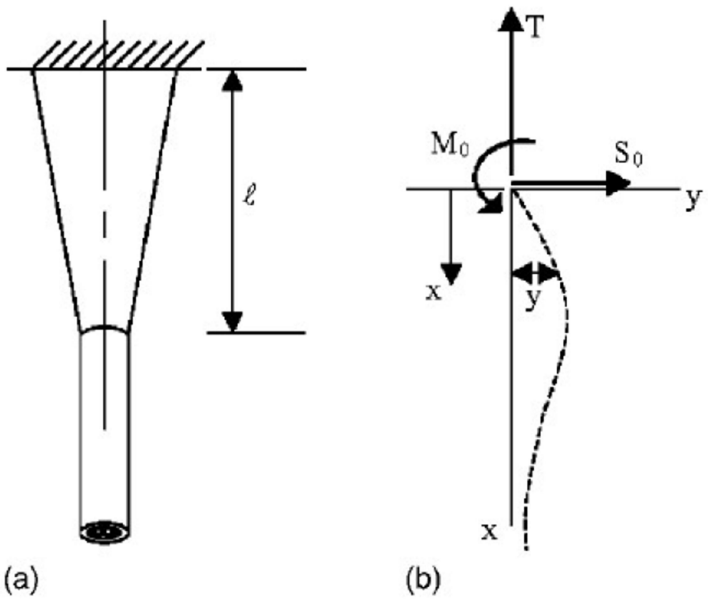

Figure 7 Diagram of TSJ and the top tensioned riser Reprinted from (Gordon et al., 2004)

The differential equations for the TSJ and the top-tensioned riser are given by

$$E\ I(x)y''(x) = Ty - \quad_o + S_0x$$

$$E\ I\ y_r''(x) = Ty_r - M_o + S_0x$$

where the *r* means the riser, T is the top tension, M_o and S_0 is the bending moment and the shear force at x=0, respectively. The solution of the differential equation for the top tensioned riser is given by

$$(x) = C_3e^{\beta x} + C_4e^{\beta x} + \frac{M_0}{T} - \frac{S_0}{T}x$$

$$\beta = \sqrt{\frac{T}{E\ I_r}}$$

The equation for the moment of inertia can be expressed as

$$I(x) = I_r \left(\frac{h-x}{a}\right)^2$$

$$h = \frac{l}{1 - \sqrt{\frac{I_r}{I_{top}}}}$$

$$a = h\sqrt{\frac{I_r}{I_{top}}}$$

where I_r is the cross sectional moment of inertia of the top tensioned riser, I_{top} is the cross sectional moment of inertia of the top of the TSJ. The differential equation for TSJ is expressed by

$$\frac{EI_r}{a^2}(h-x)^2\frac{d^2y}{dx^2} - Ty = S_0x - M_0$$

Assume that the solution is given by

$$y(x) = y_p(x) + y_c(x)$$

$$y_p(x) = \frac{M_0}{T} - \frac{S_0}{T}x$$

Determine the complementary solution as following.

$$\gamma^2 = \frac{a^2T}{EI_r}$$

$$(h-x)^2\frac{d^2y}{dx^2} + \gamma^2 y = 0$$

Assume the independent variable conversion and differentiate it.

$$h - x = e^z$$

$$-dx = e^z dz$$

$$\frac{dz}{dx} = -\frac{1}{e^z}$$

$$\frac{dy}{dx} = \frac{dy}{dz}\frac{dz}{dx} = -\frac{1}{e^z}\frac{dy}{dz}$$

$$\frac{d^2y}{dx^2} = -\frac{1}{e^{2z}}\left(\frac{d^2y}{dz^2} - \frac{dy}{dz}\right)$$

$$(\mathrm{h} - \mathrm{x})^2 = e^{2z}$$

Thus, the differential equation for the TSJ become

$$\frac{d^2y}{dz^2} - \frac{dy}{dz} - \gamma^2 y = 0$$

Assume

$$\mathrm{y} = \mathrm{Ce}^{\mathrm{Dz}}$$

and substitute the equation to the differential equation of the TSJ.

$$(\mathrm{D}^2 - D - \gamma^2)Ce^{Dz} = 0$$

$$D_{1.2} = \frac{1}{2}\left(1 \pm \sqrt{1 + 4\gamma^2}\right)$$

The complementary solution become

$$y_c(x) = C_1 e^{D_1 z} + C_2 e^{D_2 z} = C_1(h - x)^{D_1} + C_2(h - x)^{D_2}$$

Solving the differential equation for the TSJ,

$$y(x) = C_1(h - x)^{D_1} + C_2(h - x)^{D_2} + \frac{M_0}{T} - \frac{S_0}{T}x$$

The boundary conditions for the TSJ system

$$y(0) = 0, \qquad y'(0) = \theta$$

$$y(L) = 0, \qquad y'(L) = 0$$

$$y(l) = y_r(l), \qquad y'(l) = \mathrm{y}'_{\mathrm{r}}(l)$$

As a result, the bending moment and stress are given by

$$\mathrm{M_b}(x) = Ty(x) + S_0 x - M_0$$

$$\sigma_b(x) = \frac{M_b(x)c(x)}{I(x)}$$

$$\sigma_{r,b}(x) = \frac{M_b(x)c}{I_r}$$

Total stress can be determined as the sum of the bending stress and the tensile stress in the axial direction as follows:

$$\sigma_{total}(x) = \sigma_b + \sigma_{TT}$$

where σ_{TT} is the tensile stress at the section due to the applied top tension.

2.1.2 Recommended Design Criteria of TSJ in Offshore Industry

For the industrial application of the TSJ, the design of TSJ should follow the industrial standard like API Standard series. API Standard 2RD includes all design load requirements for the offshore risers design. API mainly suggests the stress-based approach to the structural analysis of the riser. Based on this suggestion, the TSJ in real-world engineering is usually designed following this stress-based approach.

To this end, the von Mises stress of the structure should be less than the maximum allowable stress of the material, which mainly includes the yield stress. The following quotation is taken from the section 5.2.3.1 in the API Standard 2RD (API, 2009):

> *The von Mises equivalent stresses should be less than the allowable stress defined by the right hand side of the following inequalities.*

$$(\sigma_p)_e < C_f \sigma_a$$

where $\sigma_a = C_a\sigma_y$, $C_a = \frac{2}{3}$ is the allowable stress factor, σ_y is the yield strength, and C_f is the design case factor.

The design case factor C_f is given by Table 2.

Table 2 Design Matrix for Rigid Risers Reprinted from (API, 2009)

Environmental Condition	C_f
Operating	1.0
Extreme	1.2
Survival	1.5

As for the boundary conditions of the TSJ system, it is assumed that the motion of the TSJ follows the motion of the platform. The motion of the platform is divided into two types: Translation and rotation. Translation is the linear motion in the x, y, and z direction as shown in Figure 8. Rotation is the movements around the x, y, and z axes as shown in Figure 8.

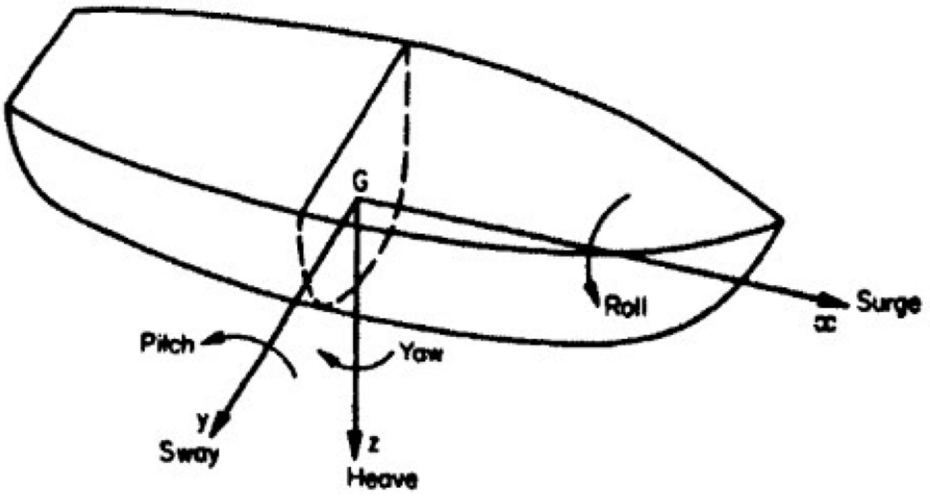

Figure 8 Ship motions Reprinted from (Tupper et al., 2001)

To discuss the boundary conditions of the TSJ system, this thesis it is assumed that the spar platform is mainly subjected to the rotation. Even though the spar platform naturally experiences both the translation and the rotation, the largest bending moment and stress is expected to occur in the rotation. When considering that the purpose of the TSJ is to reduce the bending stress level at the hang-off point, it seems reasonable to focus on the rotation so that the bending stress of the TSJ is analyzed properly.

Since the three movements of the rotation, this thesis will focus on the roll which refers to the offset or deviation from normal on the vertical axis called list or heel. These two types of the roll are actually specified according to the causes of their occurrences; however, this thesis will not discuss this in detail. Rather, this thesis will just focus on the roll itself for the implementation of the clear boundary conditions.

There are no strict criteria or standard about the degree of roll, however, the maximum value of the roll which is typically used in the analysis of the Gulf of Mexico (GOM) spar platform. The value of the maximum angle of roll that is allowable for the platform varies by three design conditions as shown in Table 3.

Table 3 Spar Motion Maximum Roll (Chang et al., 2010)

Design Condition	Case	Maximum Degree of Roll (°)
Operation	10 year hurricane	5.1
Extreme	50 year hurricane	7.8
Survival	1000 year hurricane	12.5

2.2 Finite Element Method

Finite element (FE) method is a numerical method for solving complex engineering problems such as structural analysis, heat transfer or mass transport. The FE method is particularly useful to solve the complex nonlinearity like geometry nonlinearity or material nonlinearity. Therefore, it is important to utilize the FE method to accurately simulate 3-D SMA behavior. In the FE method, several types of governing equations are required to analyze the behavior of the FE model and obtain the approximated solution.

The following sections 2.2.1 and 2.2.2 will review the constitutive models for the elastic materials and SMA. The steps of finite element method and the related framework for this thesis will be discussed in Section 2.2.3.

2.2.1 Constitutive Model for Linear Elastic Materials

Constitutive equation of elastic materials in the Cartesian coordinates, which indicates a stress-strain relation becomes (Reddy, 2004)

$$\begin{Bmatrix} \sigma_{xx} \\ \sigma_{yy} \\ \sigma_{zz} \\ \sigma_{xy} \\ \sigma_{xz} \\ \sigma_{yz} \end{Bmatrix} = \begin{bmatrix} c_{11} & c_{12} & c_{13} & 0 & 0 & 0 \\ c_{12} & c_{22} & c_{23} & 0 & 0 & 0 \\ c_{13} & c_{23} & c_{33} & 0 & 0 & 0 \\ 0 & 0 & 0 & c_{44} & 0 & 0 \\ 0 & 0 & 0 & 0 & c_{55} & 0 \\ 0 & 0 & 0 & 0 & 0 & c_{66} \end{bmatrix} \begin{Bmatrix} \varepsilon_{xx} \\ \varepsilon_{yy} \\ \varepsilon_{zz} \\ 2\varepsilon_{xz} \\ 2\varepsilon_{yz} \\ 2\varepsilon_{xy} \end{Bmatrix}$$

$$\boldsymbol{\sigma} = \mathbf{C}\boldsymbol{\varepsilon}$$

where σ is the stress, ε is the strain, and matrix C can be expressed regarding engineering constants such as the elastic modulus, Poisson'a ratio, and shear modulus. In the stress matrix at the left side, the first three stress components are direct stresses, and the rest three components are shear stresses as described in Figure 9.

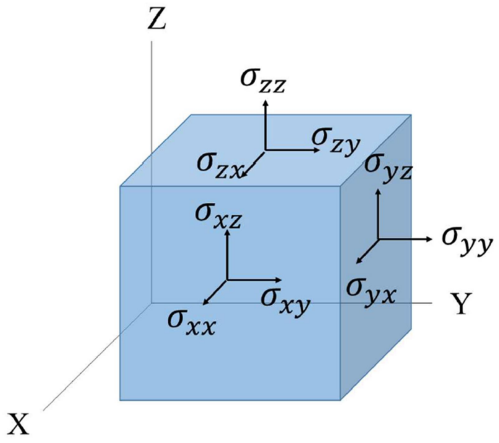

Figure 9 Cartesian stress components

2.2.2 3D SMA Constitutive Model

For the analysis of the SMA material using a finite element method, the constitutive model for SMA is required. The SMA constitutive model that will be reviewed here has been developed by Lagoudas et al. (Lagoudas et al., 2017) The total Gibbs free energy is given by

$$\mathrm{G}(\boldsymbol{\sigma}, \mathrm{T}, \xi, \boldsymbol{\varepsilon^t}) = -\frac{1}{2\rho}\boldsymbol{\sigma} : \boldsymbol{S} : \boldsymbol{\sigma} - \frac{1}{\rho}\boldsymbol{\sigma} : [\boldsymbol{\alpha}(T - T_0) + \boldsymbol{\varepsilon^t}] + c\left[(T - T_0) - T\ln\left(\frac{T}{T_0}\right)\right] - s_0 T + u_0 + \frac{1}{\rho}f(\xi)$$

where $\boldsymbol{\sigma}$ is the Cauchy stress tensor, $\boldsymbol{\varepsilon^t}$ is the transformation strain tensor, ξ is the martensite volume fraction, T is the current temperature, T_0 is the reference temperature, $f(\xi)$ is the transformation hardening function. $\boldsymbol{S}$, $\boldsymbol{\alpha}$, ρ, c, s_0 and u_0 are the material constants which refer for the effective compliance tensor, effective thermal expansion tensor, density, effective specific heat, effective entropy at reference state and effective

specific internal energy at reference state. By the rule of mixtures these material constants are defined as follows:

$$\mathbf{S}(\xi) = \mathbf{S^A} + \xi(\boldsymbol{S^M} - \boldsymbol{S^A}) = \boldsymbol{S^A} + \xi\Delta S$$

$$\boldsymbol{\alpha}(\xi) = \boldsymbol{\alpha^A} + \xi(\boldsymbol{\alpha^M} - \boldsymbol{\alpha^A}) = \boldsymbol{\alpha^A} + \xi\Delta\alpha$$

$$\mathrm{c}(\xi) = \mathrm{c}^{\mathrm{A}} + \xi(\mathrm{c}^{M} - \mathrm{c}^{A}) = \mathrm{c}^{A} + \xi\Delta\mathrm{c}$$

$$s_0(\xi) = {s_0}^{\mathrm{A}} + \xi({s_0}^{M} - {s_0}^{A}) = {s_0}^{A} + \xi\Delta s_0$$

$$u_0(\xi) = {u_0}^{\mathrm{A}} + \xi({u_0}^{M} - {u_0}^{A}) = {u_0}^{A} + \xi\Delta u_0$$

where the superscripts A and M refers for the austenite and the martensite phases, respectively. The total strain equation is given by

$$\boldsymbol{\varepsilon} = -\rho\frac{\partial G}{\partial \sigma} = \boldsymbol{S} : \boldsymbol{\sigma} + \boldsymbol{\alpha}(T - T_0) + \boldsymbol{\varepsilon^t}$$

where ε is the strain tensor, $\varepsilon^{th}$is the thermoelastic strain, and $\boldsymbol{\varepsilon^t}$ is the transformation strain tensor. The martensite volume fraction ξ is given by

$$\dot{\boldsymbol{\varepsilon}}^{\boldsymbol{t}} = \boldsymbol{\Lambda}\dot{\xi}$$

where $\boldsymbol{\Lambda}$ is the transformation tensor to determine the transformation strain direction. The transformation tensor $\boldsymbol{\Lambda}$ for proportional loading case (e.g., uniaxial loading) is expressed by two different forms as follows:

$$\Lambda = \begin{cases} \frac{3}{2}\boldsymbol{H^{max}}\frac{\sigma'}{\bar{\sigma}'} \; ; \; \dot{\xi} > 0 \\ \boldsymbol{H^{max}}\frac{\varepsilon^{t-r}}{\bar{\varepsilon}^{t-r}} \; ; \; \dot{\xi} < 0 \end{cases}$$

where H^{max} is the maximum uniaxial transformation strain and ε^{t-r} is the transformation strain at the reverse transformation. $\sigma', \bar{\sigma}'$ and $\bar{\varepsilon}^{t-r}$ are given by

$$\boldsymbol{\sigma}' = \boldsymbol{\sigma} - \frac{1}{3} tr(\boldsymbol{\sigma})\boldsymbol{I}\,, \quad \bar{\sigma}' = \sqrt{\frac{2}{3}}\|\boldsymbol{\sigma}'\|, \quad \bar{\varepsilon}^{t-r} = \sqrt{\frac{2}{3}}\|\varepsilon^{t-r}\|$$

The thermodynamic force is expressed in conjunction with the martensite volume fraction ξ as follows:

$$\pi(\sigma, \mathrm{T}, \xi) = \boldsymbol{\sigma} : \boldsymbol{\Lambda} + \frac{1}{2}\boldsymbol{\sigma} : \Delta\boldsymbol{S} : \boldsymbol{\sigma} + \boldsymbol{\sigma}$$

$$: \Delta\boldsymbol{\alpha}(T - T_0) + \rho\Delta c\left[(T - T_0) - T\ln\left(\frac{T}{T_0}\right)\right] - \rho\Delta s_0 T - \rho\Delta u_0$$

$$- \frac{\partial f}{\partial \xi}$$

The prefix Δ indicates the difference of a quantity between the austenite and the martensite phases. The material constants with the prefix Δ are given by

$$\Delta\boldsymbol{S} = (\boldsymbol{S^M} - \boldsymbol{S^A})$$

$$\Delta\boldsymbol{\alpha} = (\boldsymbol{\alpha^M} - \boldsymbol{\alpha^A})$$

$$\Delta c = (c^M - c^A)$$

$$\Delta s_0 = ({s_0}^M - {s_0}^A)$$

$$\Delta u_0 = ({u_0}^M - {u_0}^A)$$

The transformation function Φ is defined as a function of the thermodynamic force π as follows:

$$\Phi = \begin{cases} \pi - Y\,; & \dot{\xi} > 0\ (A \to M) \\ -\pi - Y\,; & \dot{\xi} < 0\ (M \to A) \end{cases}$$

where Y indicates the internal dissipation due to the phase transformation. The transformation function Φ satisfies the following condition experiencing both forward and reverse phase transformation.

$$\Phi = 0$$

The evolution of the martensite volume fraction is constrained by the following constraints that are expressed in terms of the Kuhn-Tucker conditions.

$$\dot{\xi} \geq 0, \qquad \Phi(\boldsymbol{\sigma}, \mathrm{T}, \xi) = \pi - Y \leq 0; \qquad \Phi\dot{\xi} = 0;$$

$$\dot{\xi} \leq 0, \qquad \Phi(\boldsymbol{\sigma}, \mathrm{T}, \xi) = -\pi - Y \leq 0; \qquad \Phi\dot{\xi} = 0;$$

During phase transformation, the stress and the temperature should remain on the transformation surface. This condition is expressed explicitly as follows:

$$\dot{\Phi} = \frac{\partial \Phi}{\partial \sigma} : \dot{\sigma} + \frac{\partial \Phi}{\partial T}\dot{T} + \frac{\partial \Phi}{\partial \xi}\dot{\xi} = 0$$

The transformation hardening function $f(\xi)$ is given by

$$f(\xi) = \begin{cases} \frac{1}{2}\rho b^M \xi^2 + (\mu_1 + \mu_2)\xi; & \dot{\xi} > 0 \\ \frac{1}{2}\rho b^A \xi^2 + (\mu_1 + \mu_2)\xi; & \dot{\xi} < 0 \end{cases}$$

where the b^M, b^A, and μ_1 are the material constants. μ_2 is introduced to enforce continuity for the function $f(\xi)$ during forward and reverse transformation.

2.2.3 Numerical Implementation of Constitutive Model via FE Method

The FE method is integrated with the numerical implementation of 3D SMA constitutive models for the analysis of SMA application. The numerical implementation of the SMA constitutive equations is done by FORTRAN coded subroutine. The subroutine utilizes the return mapping algorithm for the numerical implementation of the constitutive model. Using the return mapping algorithm, the subroutine results in a set of nonlinear algebraic equations, which are solved using Newton's iteration method

(Qidwai et al., 2008). Before introducing the algorithms and iteration procedure, the brief review about the FE method will be preceded for the better understanding of them.

The governing equations of the FE methods and the process of the FE analysis will be discussed here. Regarding the FE analysis, the most notable difference between the elastic materials and SMA is the material nonlinearity. As mentioned earlier, the finite element method is an efficient way to solve the nonlinearity. The FE method proceeds according to the following steps (Reddy, 2004).

Three types of governing equations are required to begin the finite element method: strain-displacement equation, the equation of motion, and constitutive equation. Strain-displacement equation in vector form is given by

$$\boldsymbol{\varepsilon} = \mathbf{D}\mathbf{u}$$

$$\boldsymbol{\varepsilon} = \begin{Bmatrix} \varepsilon_{xx} \\ \varepsilon_{yy} \\ \varepsilon_{zz} \\ 2\varepsilon_{xz} \\ 2\varepsilon_{yz} \\ 2\varepsilon_{xy} \end{Bmatrix}, \mathbf{D}^{\mathbf{T}} = \begin{bmatrix} \partial/\partial x & 0 & 0 & \partial/\partial z & 0 & \partial/\partial y \\ 0 & \partial/\partial y & 0 & 0 & \partial/\partial z & \partial/\partial x \\ 0 & 0 & \partial/\partial z & \partial/\partial x & \partial/\partial y & 0 \end{bmatrix}$$

where $\boldsymbol{\varepsilon}$ is the strain tensor, $\mathbf{D}$ is the partial matrix, and $\mathbf{u}$ is the displacement vector.

Equations of motion become

$$\mathbf{D}^{\mathbf{T}}\boldsymbol{\sigma} + \boldsymbol{f} = \rho\ddot{\boldsymbol{u}}$$

where $\mathbf{D}^{\mathbf{T}}$ is the partial matrix, $\boldsymbol{\sigma}$ is the stress tensor, $\boldsymbol{f}$ is the body force vector, ρ is the mass density, and $\ddot{\boldsymbol{u}}$ is the acceleration vector. When the system is static, the right-hand side of the equation can be assumed zero. The stress tensor, the body force vector, and the displacement vector can be expressed as follows:

$$\sigma = \begin{Bmatrix} \sigma_{xx} \\ \sigma_{yy} \\ \sigma_{zz} \\ \sigma_{xy} \\ \sigma_{xz} \\ \sigma_{yz} \end{Bmatrix}, f = \begin{Bmatrix} f_x \\ f_y \\ f_z \end{Bmatrix}, u = \begin{Bmatrix} u_x \\ u_y \\ u_z \end{Bmatrix}$$

The principle of virtual displacements for the three-dimensional elasticity problem can be expressed in vector form become

$$0 = \int_{\Omega_e} [(\boldsymbol{D}\delta u)^T \boldsymbol{C}(\boldsymbol{D}u) + \rho \boldsymbol{u}^T \ddot{\boldsymbol{u}}] dx - \int_{\Omega_e} (\delta \boldsymbol{u})^T \boldsymbol{f} dx - \oint_{\Gamma_e} (\delta \boldsymbol{u})^T \boldsymbol{t} d$$

where Γ_σ is a natural boundary conditions and Γ_u is an essential boundary conditions. By substituting the approximation of solution into the above equation, the FE model of a three-dimensional elastic body as follows:

$$\boldsymbol{M^e}\ddot{\Delta}^{\boldsymbol{e}} + \boldsymbol{K^e}\Delta^{\boldsymbol{e}} = \boldsymbol{F^e} + \boldsymbol{Q^e}$$

where $\boldsymbol{M^e}$, $\ddot{\Delta}^{\boldsymbol{e}}$, $\boldsymbol{K^e}$ is the stiffness matrix, $\Delta^{\boldsymbol{e}}$ is the degree of freedom (d.o.f) vector, $\boldsymbol{F^e}$ is the load vector, $\boldsymbol{Q^e}$ is the internal force. In static problem, $\mathbf{M^e}\ \ddot{\Delta}^{\boldsymbol{e}}$ goes to zero.

If the problem is nonlinear, which means that the engineering problem is described by nonlinear differential equations, the equation of the FE model described above is nonlinear and unsymmetric as follows:

$$\mathbf{K}(\Delta)\ \Delta = \mathbf{F} + \mathbf{Q}$$

where $\mathbf{K}(\Delta)$ is the assembled global stiffness matrix. In SMA finite element analysis, Δ is the vector of unknown nodal displacement containing temperatures. The global

stiffness matrices K(Δ) are the sum of the entries of the local stiffness matrices for each integration point of the FE model. To calculate these local stiffness matrices, the FE computational program like Abaqus utilizes the user material subroutines like UMAT. UMAT that will be used in this thesis is the customized subroutine developed by the Dept. of Aerospace Engineering at Texas A&M University. UMAT calculates the local stiffness matrices for each integration point at each iteration of the global Newton's method. At each increment of strain, or temperature (input), the value of the stress tensor and the tangent stiffness tensor, and the solution dependent variables (e.g., the martensite volume fraction and the transformation strain) (output) are updated by UMAT.

The tangent moduli tensors is the tensors that relate the strain and temperature increments (input) to the calculated stress increment (output). The SMA constitutive model in Section 2.2.2 is written in an incremental form as follows:

$$d\sigma = K_u : d\varepsilon + K_T dT$$

where K_u is the tangent stiffness moduli tensor and K_T is the tangent thermal moduli tensor. These two tensors are required for the execution of the global FE method. To this end, these two tensors must be derived for each of the forward and the reverse transformation. The full procedure of derivation can be found in the book of Lagoudas et al. (Qidwai et al., 2008).

For the system of algebraic and ordinary differential equations of the SMA constitutive model, it is assumed that the strain and temperature histories $\varepsilon(t) and\ T(t)$ are known for $t \in [0, \hat{t}]$. Initial conditions for ε^t and ξ at t=0 are also assumed. The evolution of equations for the transformation strain is given by

$$\varepsilon_{n+1}{}^{t} = \varepsilon_{n}{}^{t} + (\xi_{n+1} - \xi_{n})[(1-\lambda)\boldsymbol{\Lambda}_{n} + \lambda\boldsymbol{\Lambda}_{n+1}]$$

where λ ranges from 0 to 1 and time increment Δt is assumed as $\Delta t = t_{n+1} - t_{n}$. For λ=1, the equation is implemented for the set of equations and Kuhn-Tucker conditions explained in Section 2.2.2. Before the application of the return mapping algorithm on the set of equations, the transformation correction problem is be addressed and this is described in detail in the book (Qidwai et al., 2008). And then, at given increments of strain and temperature, the variables such as σ, ε^{t}, and ξ is updated to the next time step t_{n+1}. Note that this updates are consistent with the SMA constitutive model.

2.3 High Cycle Fatigue

High cycle fatigue analysis usually requires more than 10^{4} cycles to failure so that the structure is primarily subjected to the elastic deformation. In high cycle fatigue, the material behavior can be characterized by a stress-life curve (S-N curve). The stress-life curves of the materials are produced by a testing. Using this curve, the fatigue life can be determined by the number of cycles at a given stress amplitude. The stress-life curve method for life estimates is influenced by many factors like mean stress, loading frequency, or temperature. In this thesis, the influence of the mean stress must be included in the fatigue life prediction because the TSJ system is subjected to the already existed constant tension. The following section will review the various methods to consider the mean stress effect for the fatigue life prediction.

2.3.1 Fatigue Life Prediction via Stress-Life Curves

In this section, the stress-life method to predict the fatigue life of metallic materials will be reviewed. Fatigue life is defined as the number of stress cycles before

failure occurs. Fatigue life is influenced by some factors as it has been investigated in material science, but this thesis will focus on one of those factors: mean stress. Figure 10 shows the various types of stresses defined in cyclic stressing.

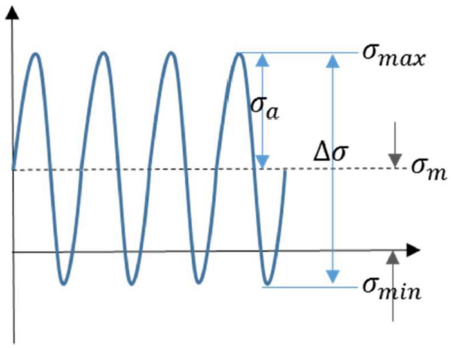

Figure 10 Cyclic stressing

where σ_a is the stress amplitude, σ_{max} is the maximum stress, σ_{min} is the minimum stress, σ_m is the mean stress. Mean stress is considered in the presence of a constant force. Since the mean stress influences the fatigue life significantly, even with the same conditions such as the same stress amplitude, it is important to consider the effects of mean stress mathematically. Various approaches to estimating mean stress effects on stress-life analysis have been researched to fit test data with superior accuracy. The modified Goodman equation using the ultimate tensile strength was suggested first and was proved that it was able to describe the elastic but it was highly inaccurate. Morrow equation using the true fracture strength made a significant improvement compared to

Goodman equation. However, the Morrow equation was found to be non-conservative for metals other than steel (Dowling, 2004). To circumvent this limitation, the Smith, Watson, and Topper (SWT) equation was developed. Walker equation is another alternative, suggesting an adjustable exponent γ. By an extension of the Morrow equation or the SWT relation, the fatigue life can be determined yet is not mathematically consistent with their parent reversed stress amplitude σ_a equations. In this work, the stress-life curves are assumed to follow a Power relationship.

$$\sigma_{ar} = \sigma'_f (2N_f)^b$$

where σ_{ar} is the reversed stress amplitude, σ'_f is a fatigue strength coefficient, N_f is cycles to failure, and b is a fatigue strength exponent. σ'_f and b are the fitting constants which are determined under the assumption of zero mean stress. The power relationship is assumed to calculate a value of completely reversed stress σ_{ar} that is expected to have the same fatigue life as the actual combination of amplitude and mean stress, σ_a and σ_m.

The reversed stress amplitude with zero mean stress σ_{ar} is assumed as a function of the stress amplitude and the mean stress with non-zero mean stress. As mentioned earlier, many researchers investigated the relation between σ_{ar} and the various stress amplitude and mean stresses and suggested various methods. Those methods vary with the type of strength that is employed in the equation.

Goodman equation includes the ultimate tensile strength as follows:

$$\sigma_{ar} = \frac{\sigma_a}{(1 - \frac{\sigma_m}{\sigma_u})}$$

However, this equation is not accurate on the life estimate so Morrow suggested modified equation as follows:

$$\sigma_{ar} = \frac{\sigma_a}{(1 - \frac{\sigma_m}{\sigma'_f})}$$

Smith, Watson, and Topper proposed new relation that will be denoted as SWT equation in this thesis. SWT equation is given by

$$\sigma_{ar} = (\sigma_{max}\sigma_a)^{\frac{1}{2}}$$

$$\sigma_{ar} = \sigma_{max}\left(\frac{1-R}{2}\right)^{1/2}$$

$$\sigma_{ar} = \sigma_a\left(\frac{2}{1-R}\right)^{1/2}$$

Dowling (2004) has done the study about the correlation of stress-life data with Goodman, Morrow, and SWT equations and concluded the followings. The Goodman equation is excessively conservative for tensile mean stresses. The Morrow equation is better than Goodman but has poor and nonconservative values for the nonferrous metals, and the SWT equation gives good results in both the ferrous and nonferrous metals (Dowling, 2004).

3. FINITE ELEMENT MODEL OF PSEUDOELASTIC SMA TSJ SYSTEM

This section now discusses the FE model of pseudoelastic NiTi TSJ system, which consists of a TSJ and an upper part of a top tensioned riser in the same fashion as Gordon's work in Section 2.1.1. The FE model will be validated by comparing the result obtained from the FE analysis to the results from Gordon's work. The following sections discuss the detailed modeling procedures.

3.1 Model Geometry

As mentioned above, the TSJ system consists of a TSJ and an upper part of a top tensioned riser. This composition of the TSJ system was derived from Gordon's work (Gordon et al., 2004). There are two main reasons why this thesis only takes the upper part of the riser into account: One is to model the system the same as Gordon's work so that the FE model can be validated. The other reason is to reduce the computation efforts for analyzing the total length of the riser since the stress distribution over the riser becomes constant beyond a certain length from the top of it. In other words, the upper part of the riser that is less than 10 % of the total length is sufficient to figure out the stress distribution over the riser and reduce the computation time. Also, this can be justified because the interest of this thesis is the TSJ, not the riser. It will be discussed further in Chapter 4.

The geometry of TSJ and the top tensioned riser model in this study is an optimized one for the elastic materials developed by Gordon as explained in Section 2.1.1. The specifications of the optimized TSJ and the riser are introduced in Table 4 and

5, respectively. TSJ is modeled to have a tapered section with a larger diameter at the top of it and the same diameter as that of the riser. The Top tensioned riser is assumed as a single tubular riser with a circular cross section.

Table 4 Top tensioned riser specification

Riser Dimensions	Value
Total Length (m)	1828
Length of the upper part (m)	121.92
Outer diameter (m)	0.3397
Wall thickness (m)	0.0122
Pipe wall density (kg/m^3)	7850

Table 5 Tapered stress joint (TSJ) specification

TSJ Dimensions	Value
Length (m)	4.572
Outer diameter (Top) (m)	0.3606
Wall thickness (Top) (m)	0.0226
Outer diameter (Bottom) (m)	0.3397
Wall thickness (Bottom) (m)	0.0122

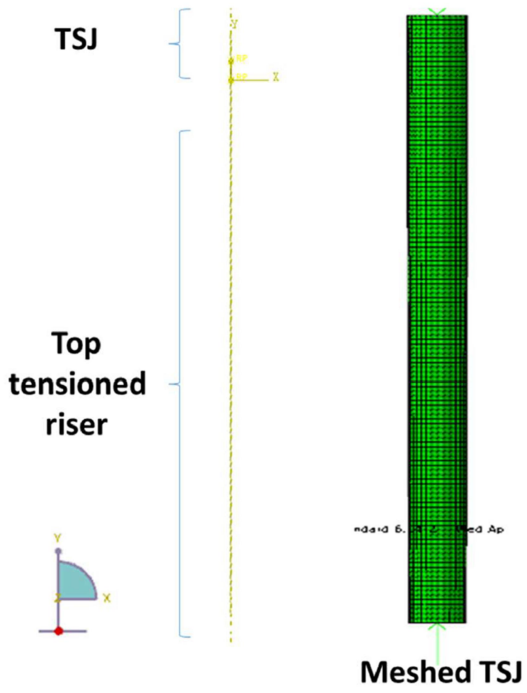

(a) (b)

Figure 11 Finite element model of TSJ system: (a) FE model of the TSJ system and (b) Meshed model of the TSJ

The FE model of the TSJ system is constructed using the Abaqus/Standard as shown in Figure 11. The TSJ model consists of quadratic solid elements with reduced integration, C3D20R, corresponding. The appropriate mesh densities were selected by running mesh convergence studies to determine the number of layers through the thickness of the TSJ in radial direction. The model determined when FEA results converge while keeping the average aspect ratio (AR) of the model at around 2:1. The top tensioned riser model consists of quadratic beam elements with reduced integration,

B32. The TSJ and the top tensioned riser in Abaqus are connected to each other by the "coupling" constraint with the "kinematic" option.

The FE model of TSJ system is validated by the results of Gordon. To this end, a distributed load was applied as the applied top tension to the top of the TSJ using " surface traction" of Load module, as shown in Figure 12. The boundary condition is given in a magnitude of 2° at the top of the TSJ. The bottom end of the TSJ system is assumed as it is fixed. The metric for comparison to Gordon's result is the maximum stress distribution over the TSJ.

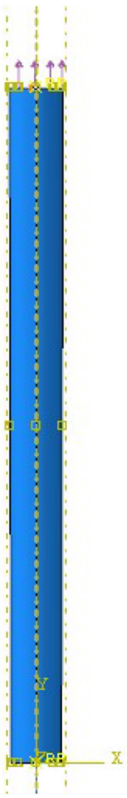

Figure 12 Applied top tension at the top of the TSJ

Figure 13(a) shows the stress distribution curves with four different outer diameter of the top of TSJ. Of the four curves, the one selected as the result of the optimization is the green line. Figure 13(b) is the maximum stress distribution curve from Abaqus FEA result. There is excellent agreement between the analytical solution result of Gordon and the FEA result. Therefore, it is confirmed that the FE TSJ model is constructed correctly. Note that 95 ksi, 85 ksi, and 95 ksi are approximately 641 MPa, 586 MPa, and 648 MPa.

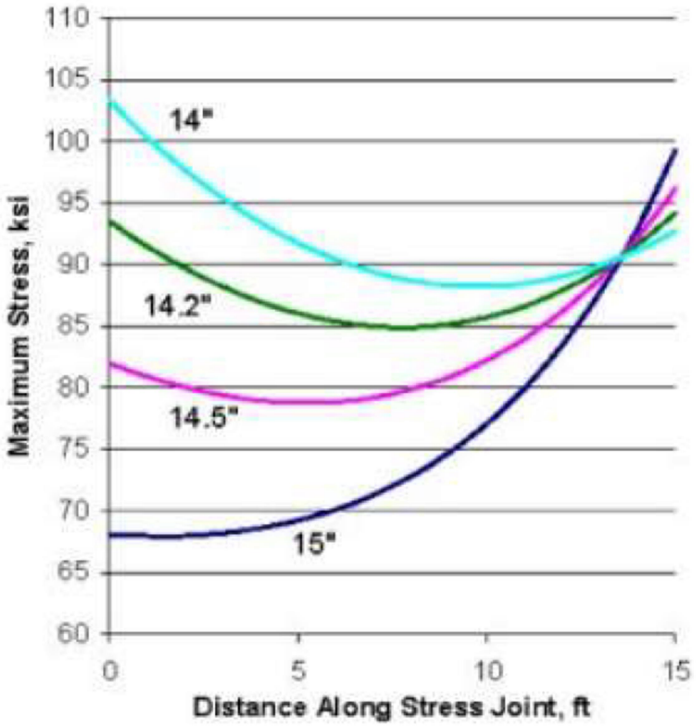

(a)

Figure 13 Comparison of (a) results of Gordon's numerical solution Reprinted from (Gordon, 2004) and (b) Abaqus FEA for validation of the FE model

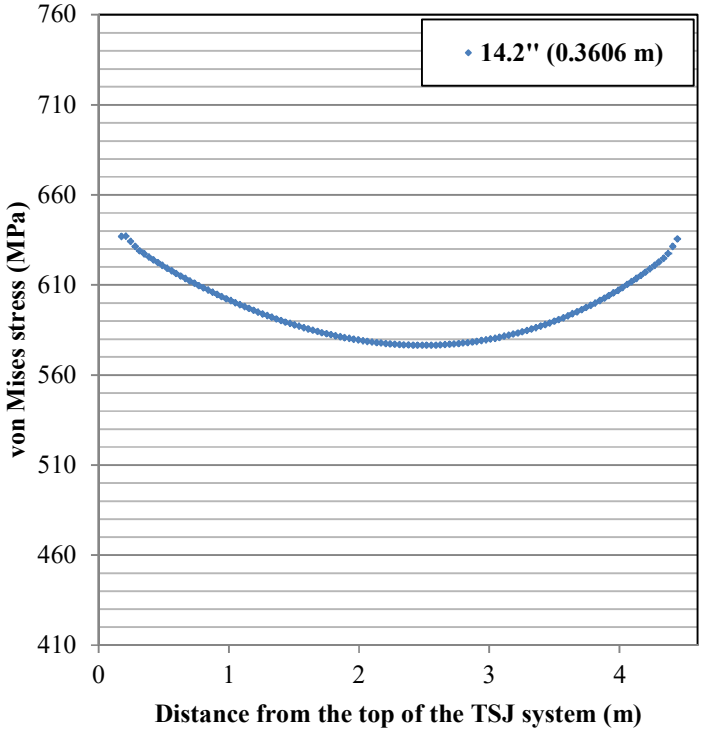

(b)

Figure 13 Continued

To investigate the advantages of applying pseudoelastic NiTi to the TSJ, two common elastic materials (i.e. steel and titanium) which are widely used in the offshore industry, were compared to Pseudoelastic NiTi TSJ. The material properties for NiTi are provided in Table 6 and those for steel and titanium are provided together in Table 7

Table 6 Material properties for NiTi shape memory alloy

Property	Value	Property	Value
ρ (kg/m^3)	6450	C_A (MPa/K)	7
E_A (GPa)	70	C_M (MPa/K)	7
E_M (GPa)	30	H_{max}	0.05
ν	0.33	n_1, n_2, n_3, n_4	0.5
$\alpha^A = \alpha^M$	22×10^{-6}		

Table 7 Material properties for steel and titanium

Property	Steel	Titanium
ρ (kg/m^3)	7850	4430
E (GPa)	210	110
ν	0.33	0.33

As for the transformation temperatures of SMA, those temperatures should be selected by considering the operating temperature of the TSJ. Temperature selection will be done in Section 3.3.

The case study of each material will be implemented to produce the more practical results. The examples of each material are selected in the ASM Handbook, which particularly has available fatigue data for a high cycle fatigue analysis. The strength and fatigue data from the book is shown in Table 8. The yield strength of NiTi

is assumed to be the 95 percent of its ultimate tensile strength. All strength data except for the yield strength of NiTi is published in ASM Handbook (ASM International Handbook Committee, 1990). The fatigue data of NiTi uses the published data of NiTi wire (Cheung, 2011). In fact, there is insufficient experimental data for the fatigue data of NiTi, and even if it is data on the wire as cited in the text, it will be possible to make further studies on it later.

Table 8 Strength and fatigue data of each material

Material		Shape Memory Alloy	Steel Alloy		Titanium Alloy
		NiTi	AISI 1018 (Carbon steels)	AISI 4130 (As-received)	Ti-6Al-4V
Yield strength (MPa)	σ_Y	912	572	778	805
Ultimate tensile strength (MPa)	σ_u	Max 960	696	895	845
Fatigue Strength coefficient (MPa)	σ'_f	705	423	1273	1293
Fatigue Strength exponent	b	-0.06	-0.07	-0.08	-0.088

3.2 Loads and Boundary Conditions

For the computational analysis of TSJ model, the type of load and boundary conditions have to be set correctly considering the type of analysis (e.g. static, quasi-static or dynamic). How and by which kind load applies to the top of the TSJ should be

determined in consideration of the type of the analysis. In this thesis, the analysis is assumed to be static analysis, implying that inertia effects and time-dependent material effects (e.g. creep, swelling, or viscoelasticity) can be neglected. According to DNV-OS-F201 standard for the offshore production, it is sufficient to implement the static analysis in the design stage of the top tensioned riser and the TSJ (DNV, 2010). Applied load in this thesis is assumed to include the weight and buoyancy of riser and the weight of internal fluid and ultimately defined as an applied top tension. The magnitude of the applied top tension to the system is calculated via analyzing the effective tension over the riser. Though there are many possible methods to this end, this thesis takes the specialized method for top tensioned riser suggested by Spark (Sparks, 2007). By using the result obtained by this method, the applied top tension is determined following the recommendation from a DNV Standard. This determination process of the applied top tension will be further discussed in the following Section 3.2.2 to show the detailed procedure and discuss the embedded physical principle in the simplified analysis.

There are two different boundary conditions: zero-displacement and a degree of rotation (roll) at the top of the TSJ and zero-displacement and zero-rotation at the bottom the riser, which means fixed end. The values for the roll angle follow the typical Gulf of Mexico (GOM) Spar motions as shown in Table 3. The boundary condition is given with the “Amplitude” option to reproduce the roll motion of the platform. Therefore, it can be assumed that TSJ rotates to the right until the given angle of rotation reaches, and then rotates to the left with the same angle of rotation. This cyclic rotation of the simulation is divided into three steps as follows (Figure 14):

- Step 1: Rotation to the right
- Step 2: Return to the initial position
- Step 3: Rotation to the left.

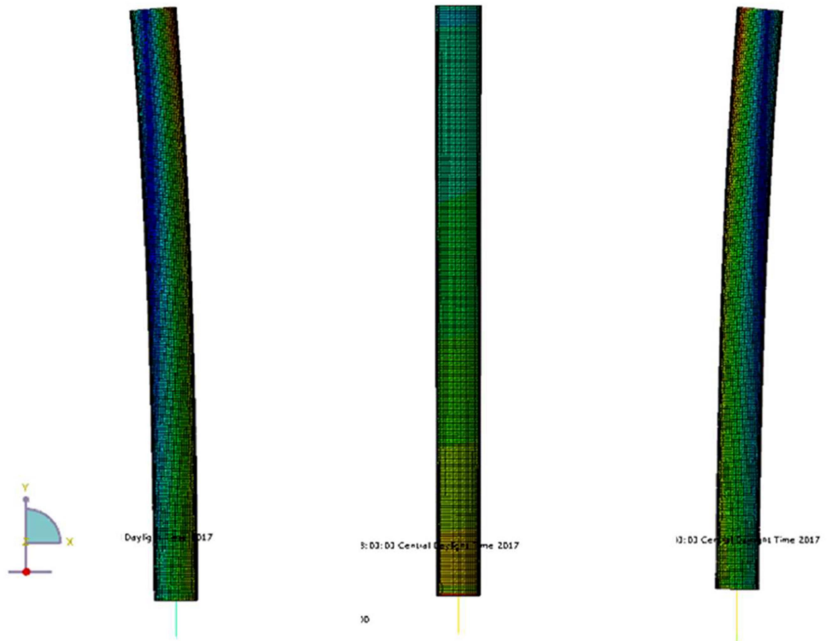

(a) (b) (c)

Figure 14 Three steps of one cyclic rotation: (a) Step 1; (b) Step 2; and (c) Step 3

In this thesis, it is assumed that the total stress is the sum at any point of the TSJ is the sum of the tensile stress in the y-direction σ_{yy} induced by the applied top tension and the bending stress σ_{bend} induced by the rotation. For the justification of this assumption, the stress components are checked to see that the stress component σ_{yy} is

highly dominant in the stress components. The stress components of one example of the FEA result are given by

$$\begin{pmatrix} \sigma_{xx} & \sigma_{xy} & \sigma_{xz} \\ & \sigma_{yy} & \sigma_{yz} \\ & & \sigma_{zz} \end{pmatrix} = \begin{pmatrix} 8 & 8 & 0.003 \\ & 532 & -0.007 \\ & & 10 \end{pmatrix}$$

where the unit of the stress is MPa. The $\sigma_{yy}$is predominantly larger than the other values because the applied top tension is sufficiently large and applied uniaxially in the y-direction. As a result, we want to denote σ_{yy} as σ_{Total}. Also, the initial tensile stress before rotation will be denoted as σ_{TT} in the sense that the tensile stress is induced by the top tension. Therefore, the total stress is given by

$$\sigma_{Total} = \sigma_{TT} + \sigma_{bend}$$

The temperature is assumed to be homogeneous over the model and also isothermal during the analysis step to mimic the pseudoelastic loading path. The temperature of the model is denoted as an operating temperature T_{op}. In this thesis, T_{op} is assumed as same as an average value of fluid temperature in the riser (357K). In the industrial practice, the fluid temperature can be characterized by the reservoir survey data.

3.2.1 Determination of the Applied Top Tension

The effective tension is obtained at any section of the riser by calculating the equilibrium of the pipe segment from the section to the top of the riser, which can be seen as an application of Archimedes law. This physical equilibrium includes the riser top tension and the apparent weight that is a net force of the gravitational force of both the pipe and the internal fluid and the buoyant force of the external fluid. In the riser

system, the internal fluid refers to the hydrocarbon, and the external fluid here refers to the seawater.

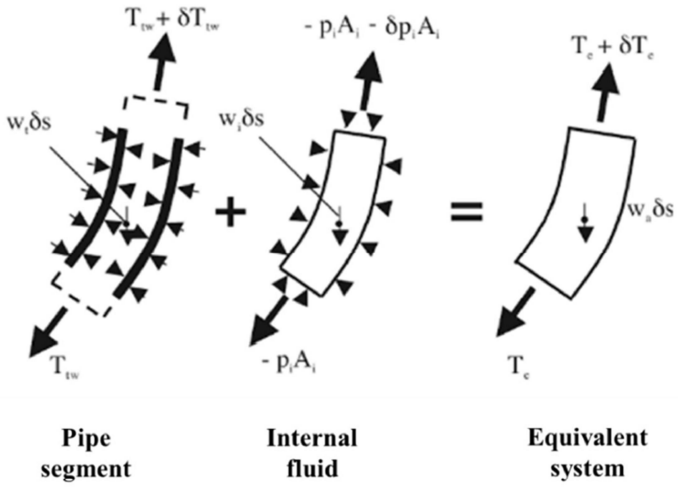

Figure 15 Pipe with interanl fluid-equivalent force systems Reprinted from (Sparks, 2007)

Figure 15 shows equivalent force systems for the case of a pipe subjected to internal pressure and the external pressure (Sparks, 2007). A pipe segment of length is assumed to be bent at an angle φ and in the equilibrium under the combined influence of pipe weight, internal pressure, external pressure, and the true wall tension acting along the pipe wall. By the addition of the force systems acting on the pipe segment (true wall tension) and the internal fluid and then the subtraction of the force system acting on the displaced fluid (seawater), all lateral pressure effects can be eliminated. The apparent

weight is simply the difference between the sum of the pipe wall weight and the internal fluid column weight and the displaced fluid column weight. The apparent weight is in equilibrium with an effective tension, a shear force and a moment. The equations for the effective tension and the apparent weight then become

$$T_e = T_{tw} + (-p_i \cdot A_i) - (-p_e \cdot A_e)$$

$$w_a = w_t + w_i - w_e$$

where T_e is the effective tension at the section, T_{tw} is the true wall tension, $p_i \cdot A_i$ is the hydrostatic force by the internal fluid, $p_e \cdot A_e$ is the hydrostatic force by the displaced fluid, w_a is the apparent weight, w_t is the pipe wall weight, w_i is the internal fluid column weight, and w_e is the displaced fluid column weight.

For the force equilibrium of the equivalent system in the axial direction, the equation of the relation between the effective tension and the apparent weight with consideration of the pipe deflection angle φ become

$$\frac{d(T_e)}{ds} = w_a \cdot \cos(\varphi)$$

If the pipe is operated vertically like top tensioned riser, above equation become

$$\frac{d(T_e)}{ds} = w_a$$

In principle, Archimedes' law can be applied directly only to completely closed pressure field. The closed pressure field combined with the distributed weight of the displaced fluid produces no resultant moment. The fluid would not be able to support the associated stresses. Since for any fluid the combined effects of its weight and enclosed pressure field can produce no resultant moment anywhere, the bending effects of forces

on the equivalent system are precisely the same as those on the pipe segment. Therefore, the simplest way to take into account the effects of internal and external pressure on pipe or riser curvature, deflection, and stability is to use effective tension and apparent weight in the corresponding top tensioned riser. Note that the effective tension equation in this section integrates the effect of pressures on a perfectly cylindrical elastic tube or pipe which undergoes small deflection. The general operation of the top tensioned riser assumes a circular uniform cross-section with small deflection. Furthermore, the top tensioned riser is assumed to be manufactured of steel, and the material is assumed to be elastic.

In summary, the concept of the effective tension can be applied to the general operating simulation of the top tensioned riser. With the specification of the top tensioned riser determined in Section 3.1, the effective tension distribution along the riser is calculated as shown in Figure 16.

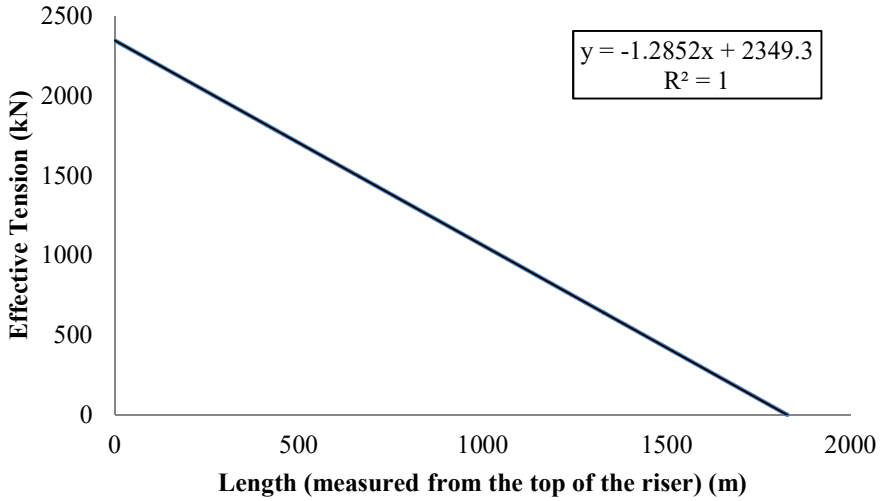

Figure 16 Effective tension distribution along the top tensioned riser

Effective tension has a maximum value of 2349.3 kN at the top of the riser having the same magnitude with the total amount of the apparent weight of the riser. The effective tension at the top of the riser system becomes lower bound of the applied top tension that is applied at the top of the riser in real case (DNV, 2010). To ensure that the applied top tension can hold the top tension riser without the compression or buckling of the riser and the collision in other riser arrays and limit the mean angles in the bottom of the risers, additional top tension should be considered as an upper limitation of the applied top tension. This increase about the effective tension at the top of the riser system is denoted as overpull (DNV, 2010). According to the DNV standard, the commonly accepted amount of overpull is determined with a typical range of 30%-60% of the effective tension at the top of the riser. This thesis takes the average of the range, 45%, therefore, the applied top tension is the sum of the overpull and the effective top

tension at the top of the riser. As a result, the applied top tension is finally determined to be 3410 kN. This determined applied top tension will be applied to the top section of the TSJ using a “surface traction” load type in a Load module of Abaqus as shown in Figure 12.

3.3 Selection of Transformation Temperatures of Pseudoelastic NiTi SMA

As discussed in Section 3.1, the transformation temperatures of SMA should be selected by considering the operating temperature of the TSJ regarding maximizing its fatigue life. The pseudoelastic effect of SMA includes inelastic deformation and the smaller the stress amplitude that occurs during a loading cycle, the more beneficial to its fatigue life. To this end, the phase diagram of the NiTi as shown in Figure 17 should be considered first. In pseudoelastic effect, the forward transformation has to start at the martensite start stress, and the reverse transformation has to end at the austenite finish stress. The TSJ model is assumed that the stress Since the TSJ model is initially subjected to the applied top tension so the initial tensile stress already exists in uniaxial direction over the TSJ even before rotation. Note that the tensile stress is distributed differently depending on the length of TSJ. The maximum initial tensile stress $\sigma_{TT,max}$ occurs at the bottom of the TSJ because the cross-sectional area at the bottom is the smallest. As shown in Figure 17, the maximum initial tensile stress should be less than the austenite finish stress of NiTi to complete the pseudoelastic effect after the completion of one rotation cycle. As a result, $\sigma_{TT,max}$ should be the lower bound of the austenite finish stress and the austenite finish temperature A_f is determined by the operating temperature T_{op} using phase diagram as shown in Figure 17. In the following

analysis, we assume that the phase diagram consists of lines, whereas in reality the phase diagram contains some curvature. Considering the safe engineering application, approximately 7 MPa margins corresponding to 1 K below T_{op} are given. Austenite finish temperature is calculated by

$$\sigma_{TT,max} + 7MPa = C_A(T_{op} - A_f)$$

$$A_f = T_{op} - \frac{\sigma_{TT,max} + 7MPa}{C_A} = 318\ \mathrm{K}$$

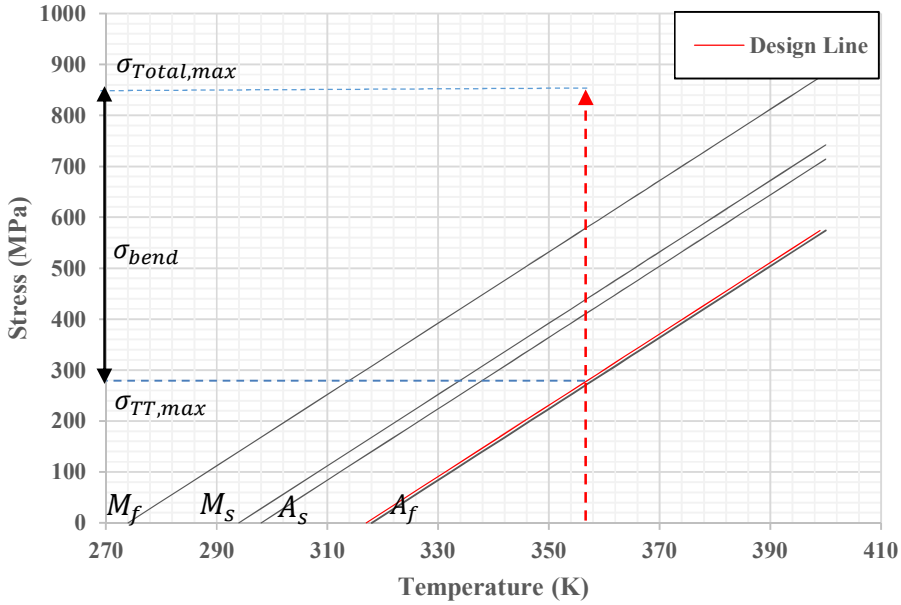

Figure 17 Phase diagram of the NiTi SMA for selecting the transformation temperatures

Other transformation temperatures like M_s, M_f, and A_s are determined successively (Table 9) using a typical gap between each temperature following one example of Lagoudas' book (Qidwai et al., 2008). The stress of each transformation is calculated linearly using C_A and C_M as shown in Table 6. Note that these selected

temperatures and stresses are applicable only with the selected geometry and the top tension.

Table 9 Selected transformation temperatures at a given operating temperature

Parameter	Value
T_{op} (K)	357
M_s (K)	294
M_f (K)	274
A_s (K)	298
A_f (K)	318

Table 10 Linearly calculated stress at each transformation temperature

Parameter	Value
σ_{Ms} (MPa)	441
σ_{Mf} (MPa)	581
σ_{As} (MPa)	413
σ_{Af} (MPa)	273

4. FINITE ELEMENT ANALYSIS OF PSEUDOELASTIC SMA TSJ SYSTEM

Based on the FE model of TSJ system in Chapter 3, FEA will be implemented to understand the TSJ system's response. The results of the analysis will help engineers to understand the advantages of the pseudoelastic NiTi SMA application to the TSJ and operate the TSJ system with the changing operating conditions. To this end, the results of FEA will be used to the stress analysis and the fatigue life analysis.

The first section will discuss the elastic and pseudoelastic response of the SMA and compare the result to the cases of the steel and titanium. The second section will discuss the results of cyclic rotation simulation to estimate the fatigue life of the TSJ via stress-life curves as explained in Section 2.3.2.

4.1 Stress Analysis Results

4.1.1 Satisfaction of Recommended Design Criteria

As discussed in Section 3.2, the FE model of TSJ system are assumed to be uniaxially loaded in the y-direction. Based on this assumption, it is also assumed that the stress in the y-direction is dominant among the components of the 3-D stress matrix.

This section will implement the stress analysis with the results obtained from the FEA of the TSJ system. The first analysis is to check that the maximum von Mises stress is less than the allowable stress. To this end, the maximum von Mises stress distribution curve is obtained as shown in Figure 18. In this analysis, the degree of rotation is given as 5.1°, which is a value corresponding to the "Operation" design condition and "10-year hurricane" case as listed in Table 3. The distance in the x-axis is measured from the top

of the TSJ so that the total distance of the TSJ system is the sum of the length of the TSJ and the top tensioned riser. Note that the stress over the riser became constant and this is why the use of only upper part of the riser is sufficient for the FE model. Note also that the stress over the TSJ is extracted from the node of each solid element on the tensioned side of the TSJ model and the stress over the top tensioned riser is extracted from the integration point of each beam element on the tensioned side of the TSJ model.

In Abaqus, the top tensioned riser is modeled with a pipe section (thin-walled) that has eight integration points (IPs). Among those eight IPs, the stress outputs are given at four IPs. These four IPs are located on the intersection of the surface with two mutually perpendicular axes across the pipe section. The maximum stress occurs at the IP that is located at the tensioned side of the riser. In Figure 18, it is shown that the steel TSJ exhibits the greatest stress among the three material studied, whereas the NiTi TSJ exhibits the smallest stress.

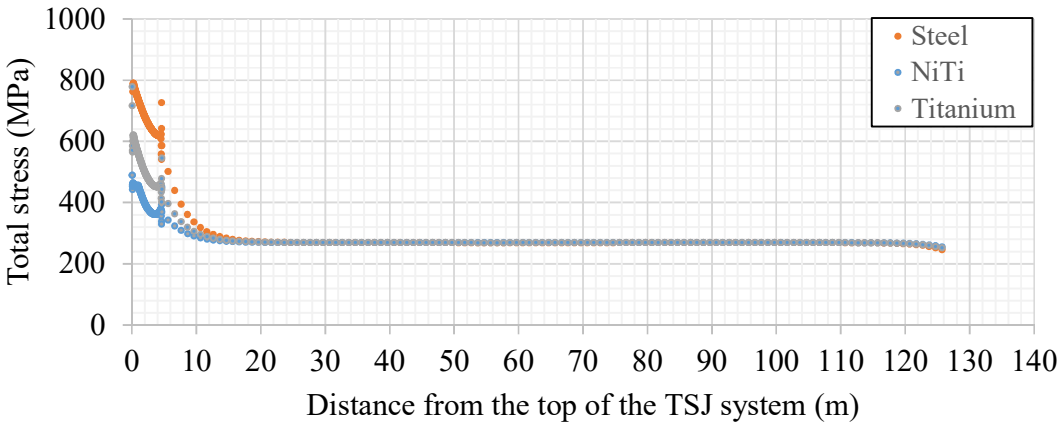

Figure 18 Stress distribution of the TSJ system

The stress distribution over the TSJ is shown in Figure 19. Notably, the stress is very high at both the top and the bottom of the TSJ. These anomalous data points are due to the constraints and interaction boundary conditions at these points. The "tie" constraint and the "rigid body" constraint were applied at the top of the TSJ. The "coupling" constraint and the "rigid body" constraint were applied at the bottom of the TSJ. This may have constrained any Poisson effects resulting in a local increase in the computed stress. Therefore, the data was post-processed by comparison with Gordon's analytical solution as shown in Figure 20 to show the maximum stress distribution over the TSJ more clearly.

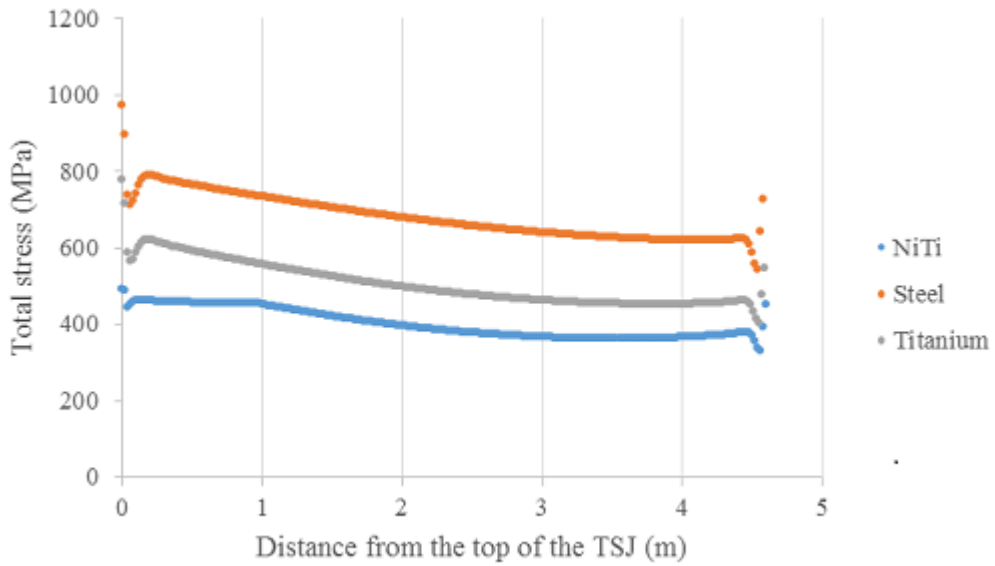

Figure 19 Stress distribution along the TSJ

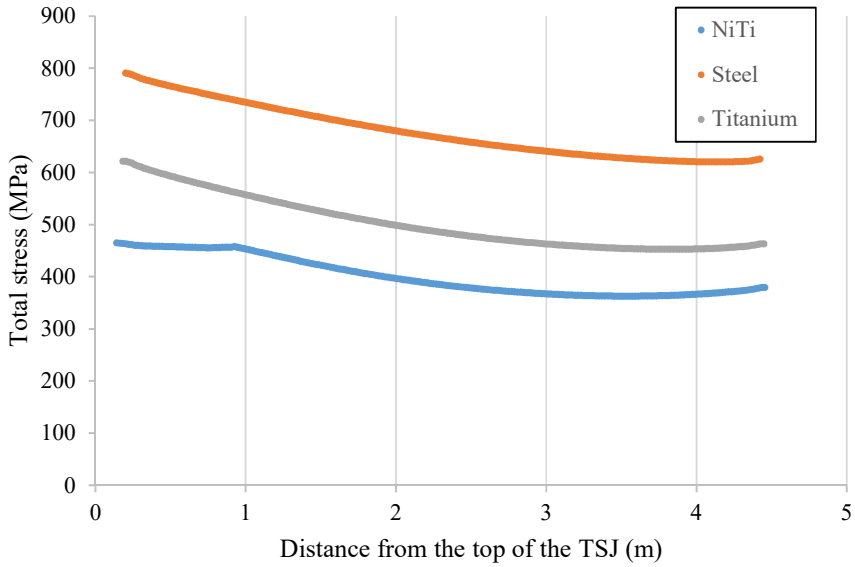

Figure 20 Stress distribution along the TSJ after post-processing

In Figure 20, the most important result here is that the lowest stress is generated in the structure to which the pseudoelastic NiTi is applied. The stress in case of the steel was the highest, followed by the titanium TSJ. Moreover, the martensite transformation can be assumed to have occurred at the upper part of the NiTi TSJ because the the stress level slightly decreased. In other words, if NiTi only deforms elastically, then the slope of the curve should be similar to the steel and titanium cases. Therefore, the FEA assuming that NiTi deforms only elastically is implemented, and the result is shown in Figure 21. In Figure 21, the position in the x-axis is assumed that the data were given from the first point of the post-processed data. It is clear that the slope of NiTi curve has the same tendency as the elastic material if there was no martensite transformation. It is

also notable that the stress level of the transformed section is greater than the martensite start stress. Additionally, it is very notable that the martensite transformation reduces the stress at the top of the TSJ, called Hang-off point. This concludes that the use of a pseudoelastic NiTi TSJ not only retains the original advantage of an elastic TSJ itself but also a reduction in stress due to the phase transformation.

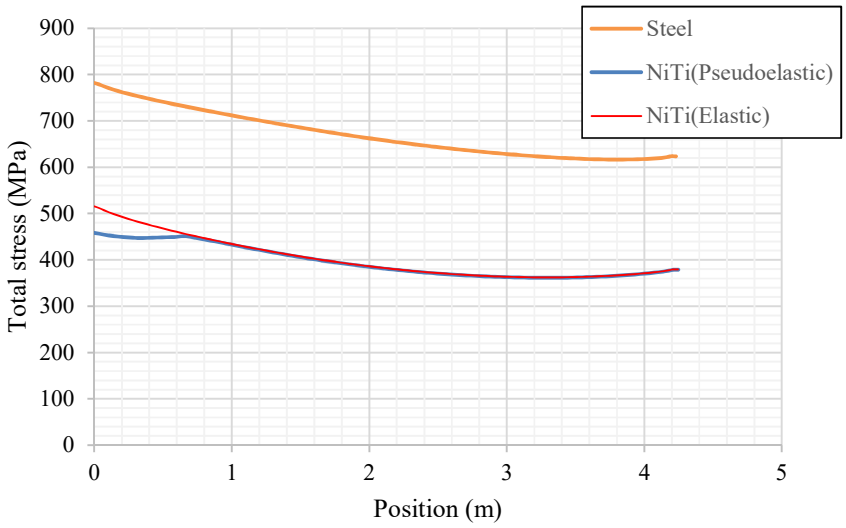

Figure 21 Comparison of the stress along the steel TSJ, the elastic, and the pseudoelastic NiTi TSJ

To check if the designed TSJ with each material is acceptable according to industry standard, the maximum stress should be compared to the allowable stress of each case. Following the design criteria in Section 2.1.2, the allowable stresses are calculated as shown in the third row of Table 11 using the yield strength data given in

Table 8. As it is assumed earlier, the von Mises stress is replaced by the total stress σ_{Total} and the result obtained by the FEA is shown in the fourth row of Table 11.

Table 11 Satisfaction of design criteria for each material case

Condition	Operating (angle of rotation=5.1 deg)			
Material	$Ni_{50}Ti_{50}$	AISI 1018 (Carbon steels)	AISI 4130 (As-received)	Ti-6Al-4V
Allowable Stress (MPa)	608	381.3	518.7	536.7
Total Stress (MPa)	464.93	791.00		621.93
Satisfaction of Criteria	Satisfied	Not Satisfied		Not Satisfied

The result shows that the pseudoelastic NiTi TSJ satisfies the design criteria, whereas both the steel and the titanium TSJ do not as shown in the fifth row of Table 11. The reason is that 5.1 degrees of the rotation angle are the limit assuming possible operation of the platform even in the situation of the 10-year hurricane. It does not experience roll motion up to 5.1 degrees during its normal operating conditions, but it is hard to expect that the steel or titanium TSJ will perform its originally intended function when the 10-year hurricane occurs. On the other hand, a pseudoelastic NiTi TSJ experiences lower stress than its allowable stress because the slope of the stress-strain curve during the martensite transformation is very small. As a result, it is reasonably expected that the pseudoelastic NiTi TSJ will satisfy the larger degree of rotation in the

cases of “extreme” and “survival.” Whether this expectation is actually met will be discussed in section 4.1.3.

4.1.2 Elastic Behavior of NiTi TSJ

Before we focus on the advantages of pseudoelastic effect on the NiTi TSJ this section will review some compelling advantages regarding the elastic behavior of NiTi TSJ, which can be obtained by the comparison to the steel and titanium TSJ. To this end, the stress analysis is implemented up to the degree of rotation, which is just before the martensite transformation initiates. The stress changes up to 5.1 degrees of rotation is shown in Figure 22. We can see that the transformation starts at the martensite start stress σ_{MS}, 441 MPa. At this martensite start stress, the degree of rotation is 4.20°.

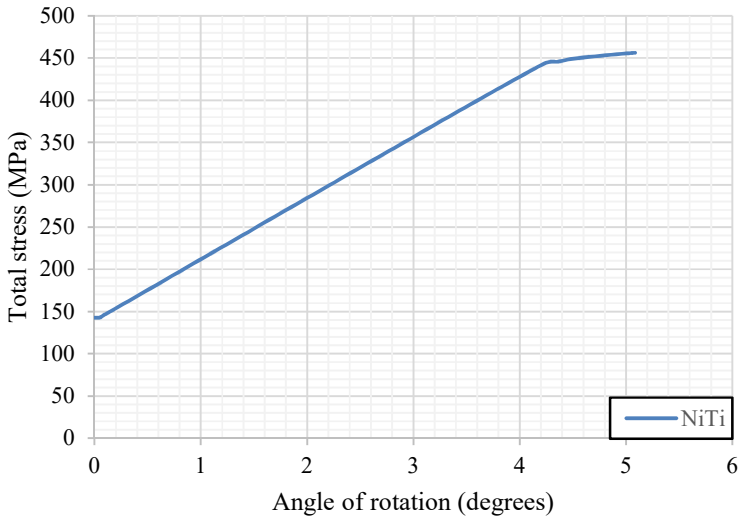

Figure 22 Total stress change by the angle of rotation

Before the degree of rotation is 4.20°, all three materials show only the elastic response. Under the assumption that there is the only elastic response, we can predict the yield angle Φ_{yield} based on the analysis of obtained elastic response of TSJ. With the elastic materials in cyclic rotation, the angle of the rotation is linearly increased by each increment of time and the bending stress increases linearly with the angle of rotation as shown in Figure 23 and Figure 24. The total stress is given by

$$\sigma_{Total} = \sigma_{TT} + \sigma_{bend} = \frac{F}{A^*} + c\Phi$$

where F is the applied top tension in y-direction at the point, A^* is a sectional area at the point, c is defined as a material property at the given temperature and the geometry of the TSJ, and Φ is an angle of rotation at the top of the TSJ. The constant c is given by

$$c = \frac{\sigma_{bend}}{\Phi}$$

where c is the slope of the bending stress-rotation curve as shown in Figure 24. The rate at which the bending stress increases by the increment of the degree denoted as c varies from material to material. Solve for Φ to find the degree of yielding, as follows:

$$\Phi_{yield} = \frac{1}{c}(\sigma_{yield} - \frac{F}{A^*})$$

where Φ_{yield} is the yield angle and σ_{yield} is the yield strength.

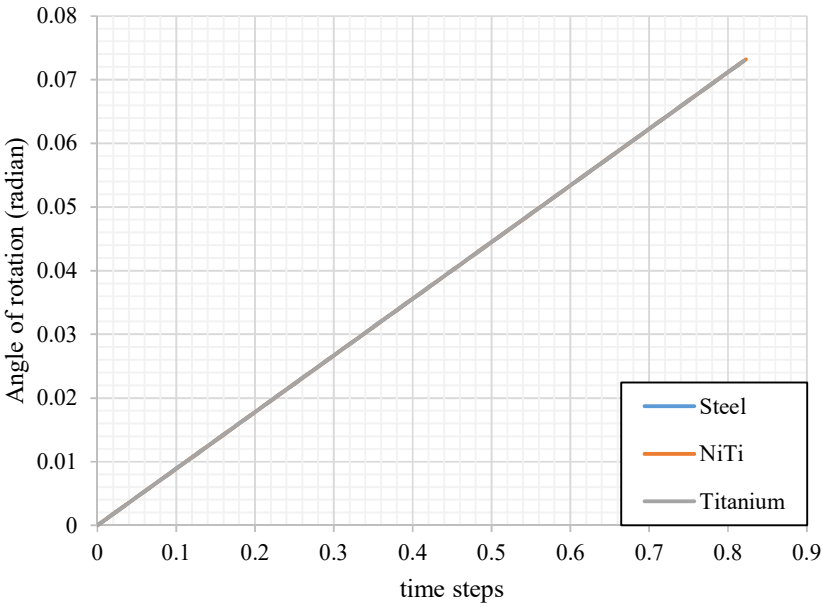

Figure 23 Change of the angle of rotation by the time

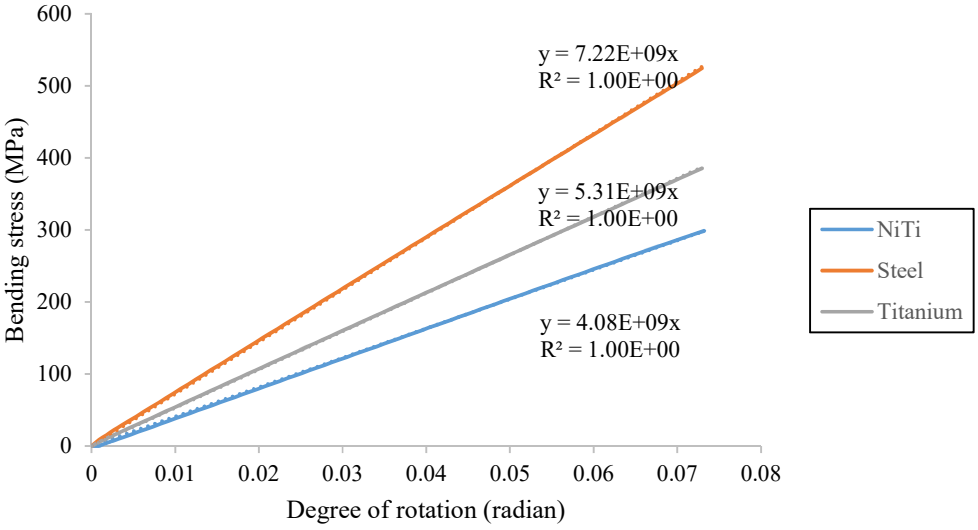

Figure 24 Change of the bending stress by the degree of rotation

Using the yield strength data in Table 8, the degree of yielding is calculated as shown in Table 12. It is clear that NiTi shape memory alloy is much beneficial than the steel and titanium alloys in terms of the rotation. Note that the yield angle of NiTi does not consider the martensite transformation. Still, the value of the yield angle Φ_{yield} of NiTi will increase much more than 10.79° if the martensite transformation considered.

Table 12 Yield angle of the TSJ with four different materials

Material	Grade	Constant c (GPa)	Φ_{yield} (°)
NiTi	Ni50Ti50	4.08	10.79
Steel	AISI 1080	7.22	3.40
	AISI 4130		5.03
Titanium	TI-6Al-4V	5.31	7.13

Finally, we can find the degree of rotation at which the martensite transformation initiates by using the shape memory alloy properties determined in Chapter 3. Since the TSJ model is assumed to be subjected to the uniaxial loading, total stress is given by

$$\sigma_{Total} = \sigma_{TT} + \sigma_{bend} = \frac{F}{A^*} + c\Phi$$

In phase diagram of SMA, the von Mises stress σ_{vM} when the martensite transformation starts is given by

$$\sigma_{vM} = C^M(T_{op} - M_s)$$

where C^M is a stress influence coefficient of the martensite SMA, T_{op} is an operating temperature, and M_s is a martensite start temperature. By combining two equations, the degree of rotation before the martensite transformation Φ_{tr} can be calculated by

$$\Phi_{\mathrm{tr}} = \frac{C^M}{c} T_{op} - \frac{1}{c}\left(C^M M_s + \frac{F}{A^*}\right)$$

The constant c is given by

$$c = \frac{\sigma_{bend}}{\Phi}$$

As a result, the angle of rotation when the martensite transformation of the TSJ initiates can be determined at a given T. As for the case study in this thesis, equation of Φ_{tr} become

$$\Phi_{\max} = 0.00175 T_{op} - 0.55025 \text{ (radian)}$$

$$\Phi_{\max} = 0.1003 T_{op} - 31.543 \text{ (degree)}$$

and this function can be briefly drawn as shown in Figure 25.

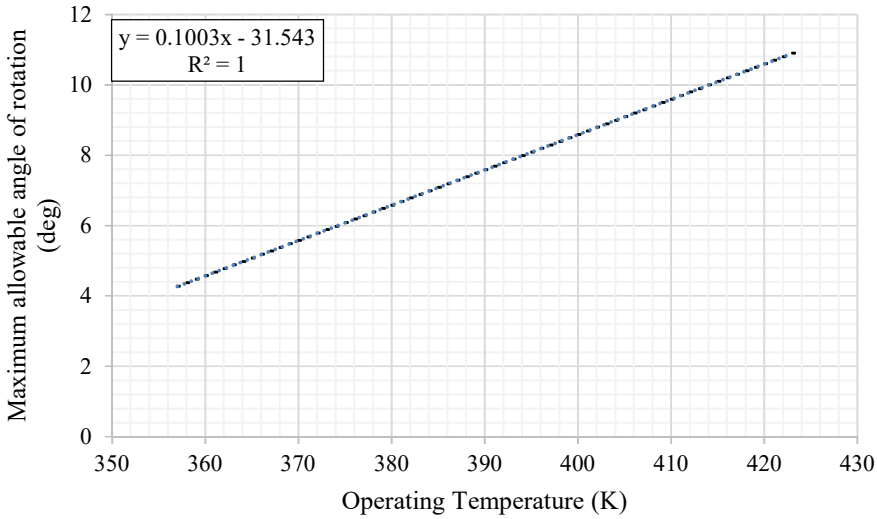

Figure 25 Degree of rotation-Operating temperature curve of NiTi TSJ

This curve allows the engineers to decide the maximum angle of rotation before the SMA TSJ experiences the martensite transformation at a given TSJ geometry and a given top tension that is applied considering the top tensioned riser which the TSJ holds. It is also interesting to note that when the when the operating temperature T_{op} rises by 1 K, the maximum allowable angle of rotation increases by about 3 degrees. When we consider that one of the imminent challenges in the offshore industry is HT fluid (High-Temperature fluid), it is beneficial to use the NiTi TSJ because the range of allowable rotation is wider as the operating temperature risers. Also, since the normal operating conditions of the Spar platform less likely to rotate much, pseudoelastic NiTi TSJ can be used much longer than the steel and the titanium TSJ.

4.1.3 Pseudoelastic Behavior of NiTi TSJ

In previous section, it is confirmed that the designed NiTi TSJ experiences the martensite transformation at the 5.1 degrees, which is corresponding to the roll angle of the 10-year hurricane. Therefore, it is obvious that the NiTi TSJ will experience a larger transformation as the roll angle increases. In this section, we will discuss the stress behavior of pseudoelastic NiTi TSJ in a cyclic rotation of the 5.1 degrees roll. Also, the more severe design conditions given in Table 3 (i.e., extreme and survival) will be analyzed to ensure that the pseudoelastic NiTi is much beneficial to the high-stress concentration.

By Abaqus/Standard with the user subroutine UMAT, the FE model of the TSJ system is analyzed. As explained earlier, the model rotates to the right and left by 5.1 degrees. In Figure 26, the results of one cyclic unit rotation with different three materials are shown. The results are extracted from the point at which the maximum stress occurs over the TSJ. For the better understanding of the stress change in a cyclic rotation, one unit cycle is divided into three periods, A, B, and C as shown in Figure 26. In section A, the TSJ rotates resulting in the increase in stress. Period B describes the TSJ coming back its original position. As the start of period C, the TSJ rotates to the left resulting in the decrease of stress due to the compression of the point.

It can be seen that the stress is large in the order of steel, titanium, and NiTi. Since the steel and the titanium are assumed to be elastic, the bending stress changes linearly by the angle of rotation. However, the response of NiTi is not linear, and slopes

are changing as seen in Figure 26. The changes in slope are due to the martensite transformation of NiTi.

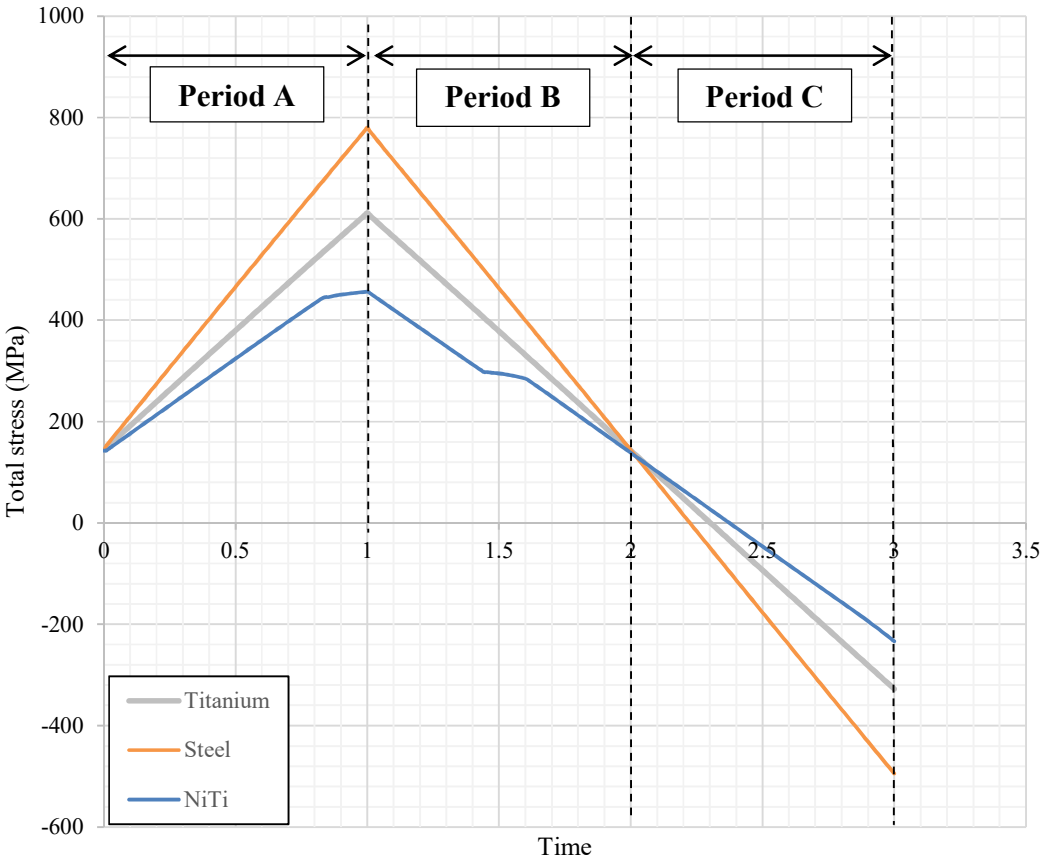

Figure 26 Cyclic stress behavior with three materials (i.e., steel, titanium, and pseudoelastic NiTi)

Figure 27 illustrates the stress change of NiTi alone to analyze the pseudoelastic behavior of TSJ. Point a means the start of the martensite transformation resulting in a notable decrease in stress growth rate, which is followed by reduction of the maximum

stress, σ_{max} at point ***b***. The stress when the slope of the curve changes is 441 MPa, and this coincides with the martensite start stress of NiTi. As returning to its original vertical position, the stress is released. When the stress level falls to the around 300 MPa denoted as point ***c***, the slope of the curve changes with a decrease in reduction rate. The slope of the curve changes again at the point c at which the stress level is 286 MPa. This number is very close to the austenite finish stress, 273 MPa with an error of 4.7 %. This change means that the phase of NiTi returns to the austenite. After the point ***d***, the slope of the curve remains same until the end of the rotation to the left.

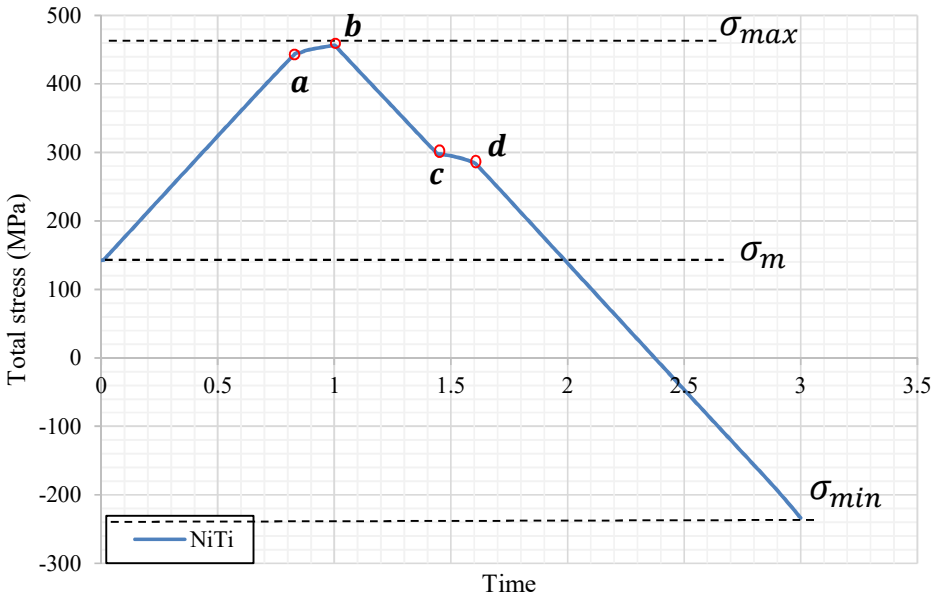

Figure 27 Change of Total stress of the pseudoelastic NiTi in a cyclic rotation

It is evident that the NiTi experiences the pseudoelastic effect and its phase changes in the following order: austenite -> martensite -> austenite. In other words, NiTi TSJ experiences complete reverse transformation as well as forward transformation. This phase transformations are intentionally designed considering the initial stress distribution due to the applied top tension as explained in Section 3.3. For confirming this hypothesis, it is reasonable to check the following three curves: the stress-strain curve, the martensite volume fraction (MVF) change curve, and the stress change curve by the degree of rotation as shown in Figure 28, 29 and 30. Figure 28 is the stress-strain curve of the NiTi in a cyclic rotation. Figure 30 illustrates how total stress changes by the degree of rotation. The hysteresis loops can be seen in both figures. Additionally, we can see that the NiTi TSJ has definitely passed both the forward transformation and the reverse transformation through the MVF curve in Figure 29. A MVF value of zero means that the material phase is austenite. Considering the fact that the value of the MVF is very small means that the NiTi transformed very little, it can be claimed that the NiTi TSJ can withstand an angle of rotation much greater than 5.1 degrees, which is the used angle of rotation in this study. That is, the NiTi TSJ can survive in extreme conditions with larger angles of rotation.

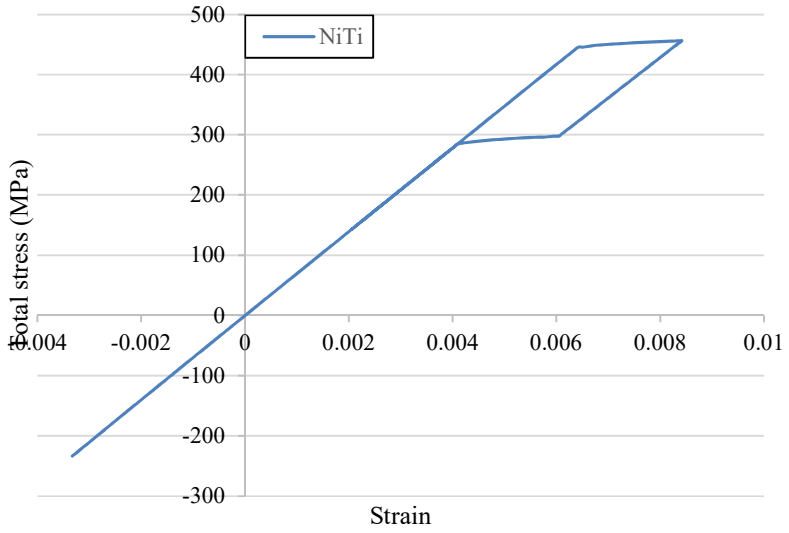

Figure 28 Stress-strain curve of the pseudoelastic NiTi TSJ

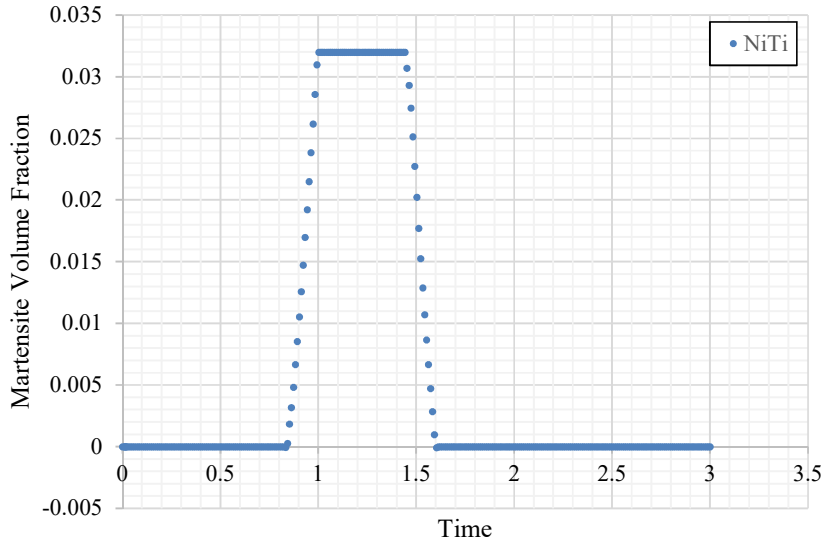

Figure 29 Martensite Volume Fraction (MVF) curve of the pseudoelastic NiTi TSJ

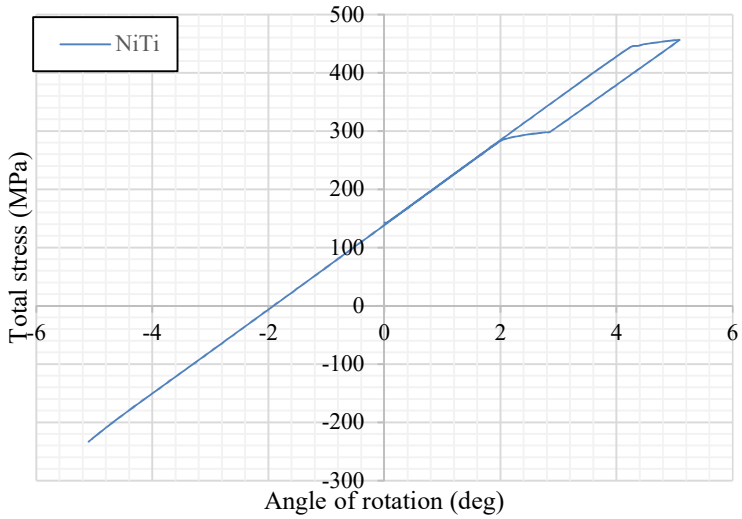

Figure 30 Change of the total stress the pseudoelastic NiTi TSJ by the angle of rotation

4.2 Fatigue Life Analysis Results

In this analysis, the fatigue life of the pseudoelastic NiTi TSJ is predicted by using two different equations as discussed in Section 2.3.1. As discussed earlier, both two equations apply to high cycle fatigue behavior that accounts for a number of cycles only about 10^5 or more. The following sections will review the equations and solve for the number of cycles that means the fatigue life.

4.2.1 Formulation of Equations for Fatigue Life Calculation

SWT equation is given by

$$\sigma_{ar} = \sigma'_f \left(N_f\right)^b = (\sigma_{max}\sigma_a)^{1/2}$$

where σ_{ar} is the reverse stress amplitude, N_f is the number of cycles, σ_{max} is the maximum stress amplitude, σ_a is the stress amplitude, σ'_f is the fatigue strength coefficient, and b is the fatigue strength exponent. Solving for N_f become

$$N_f = \frac{1}{2}\left[\frac{(\sigma_{max}\sigma_a)^{\frac{1}{2}}}{\sigma'_f}\right]^{1/b}$$

Morrow equation is given by

$$\sigma_{ar} = \sigma'_f(N_f)^b = \sigma_a\left(1 - \frac{\sigma_m}{\sigma'_f}\right)^{-1}$$

where σ_m is the mean stress. Solving for N_f become

$$N_f = \frac{1}{2}\left[\frac{\sigma_a}{\sigma'_f\left(1 - \frac{\sigma_m}{\sigma'_f}\right)}\right]^{1/b}$$

Using SWT and Morrow equation, the fatigue life N_f is calculated by the stress amplitude and the mean stress obtained from the FEA results.

4.2.2 Prediction of Fatigue Life

For estimating the fatigue life of the TSJ, the stress amplitude σ_a, maximum stress σ_{max} and the mean stress σ_m should be obtained from the FEA results. Since it is assumed that the fatigue estimates using the SWT and Morrow equations are implemented primarily with elastic deformation data, the FEA result data to be used for the fatigue life analysis is limited to that before the transformation takes place.

Figure 31 illustrates the maximum stress that occurs over the TSJ during one cycle of rotation at each angle of rotation. The study is conducted with three different

materials (i.e. steel, titanium, and NiTi). The stress is extracted from the point where the maximum stress occurs in the tensioned side of the TSJ. In section 4.1.2, it is already discussed that the maximum angle of rotation before the NiTi TSJ experiences martensite transformation is 4.20°. Therefore, the study is conducted for each angle of rotation up to 4.20°.

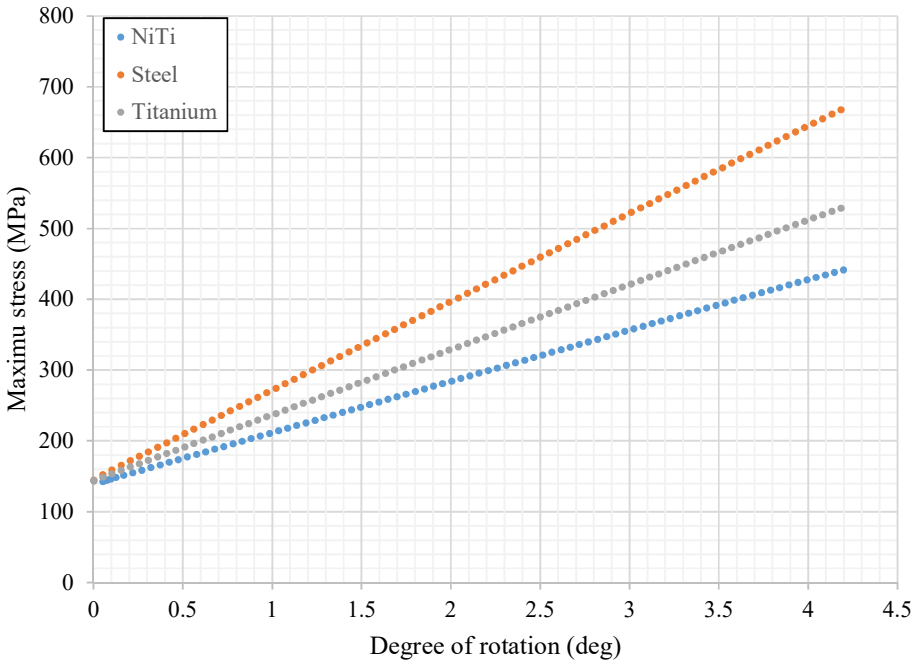

Figure 31 Maximum stress at each angle of rotation

By using the maximum stress σ_{max} obtained as shown in Figure 31, the stress amplitude σ_a is calculated as follows:

$$\sigma_a = \frac{\sigma_{max} - \sigma_{min}}{2}$$

Note that σ_{max} is the maximum stress value during one cycle of rotation at the one point. Therefore, σ_{max} is the sum of the initial tensile strength due to the top tension σ_{TT} and the increase of the bending stress due to the rotation σ_{bend}.

$$\sigma_{max} = \sigma_{TT} + \sigma_{bend}$$

The minimum stress σ_{min} occurs when the TSJ rotates to the left completely. The maximum compression occurs at the point where the maximum tension occurs. Therefore, $\sigma_{max}\ and\ \sigma_{min}$ can occur at the same point. σ_{min} is calculated by

$$\sigma_{min} = \sigma_{TT} - \sigma_{bend}$$

The stress amplitude is calculated by

$$\sigma_a = \frac{\sigma_{max} - \sigma_{min}}{2} = \frac{(\sigma_{TT} + \sigma_{bend}) - (\sigma_{TT} - \sigma_{bend})}{2} = \sigma_{bend}$$

In our FE model, the mean stress σ_m is the initial tensile stress due to the applied top tension before rotation, 142.60 MPa.

Based on the results, the fatigue life is calculated using the SWT equation and the Morrow equation. The fatigue properties refer to Table 8. The calculated fatigue life for four different materials is shown in Figure 32 and 33. These rotation-life curves apply SWT equation and Morrow equation, respectively.

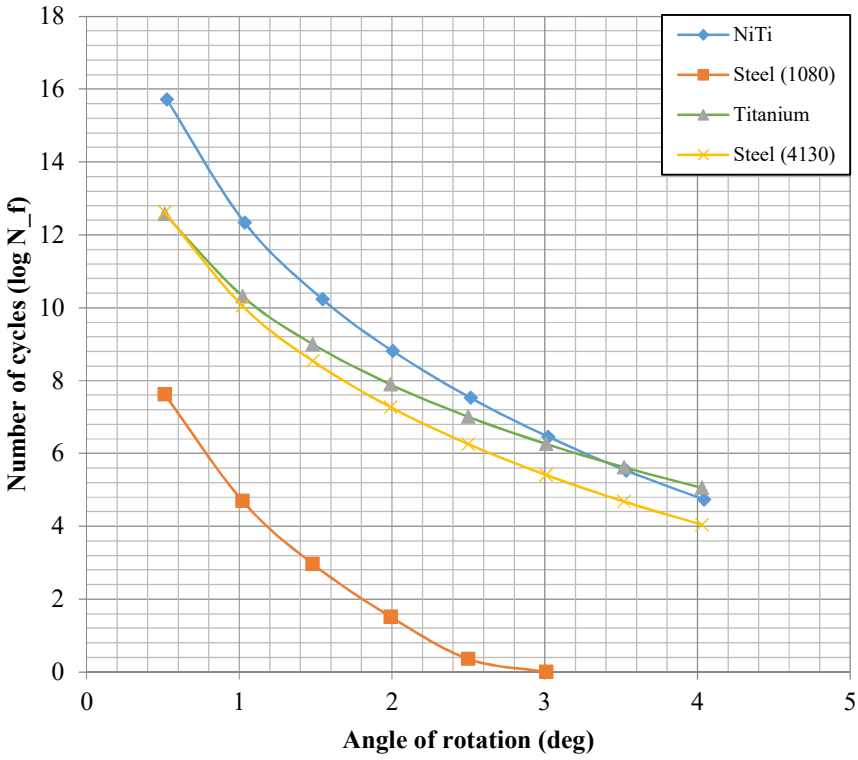

Figure 32 Rotation-Life curve using SWT Equation

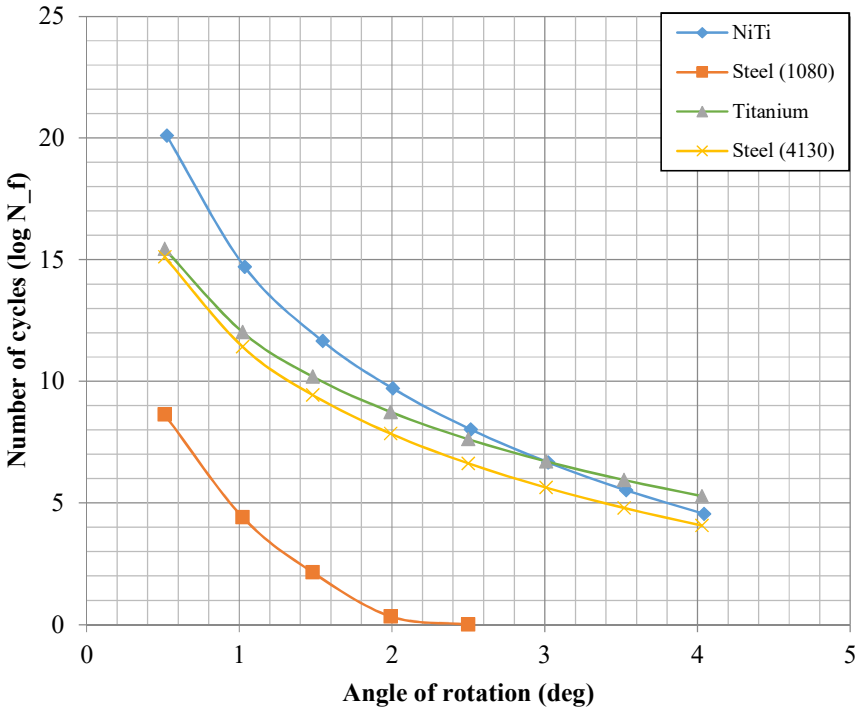

Figure 33 Rotation-Life curve using Morrow Equation

Even though different equations are applied, it can be seen that the fatigue life ranking, the difference, or the tendency to increase or decrease between the four kinds of materials is very similar. The material that has the longest fatigue life is NiTi, which is about 100,000 times the steel (AISI 4130) and titanium (TI6Al4V) alloys. This dominance is notable in a small rotation section, which is closely related to high cycle fatigue with a relatively small stress amplitude. The fact that the fatigue life of the titanium alloy TSJ exceeds that of the NiTi in a relatively large angle $(3° - 4.2°)$ suggests that the NiTi alloy should be carefully reexamined taking into account more accurate fatigue data and plastic strain-life relation. As discussed earlier, the SWT and Morrow equations do not consider inelasticity. The equations only consider the stress

amplitude, mean stress, and the stress-related fatigue data, which is decided from the analysis of the experimental data using the elastic strain-life relation. Still, it is apparent that the SMA is more useful material for the TSJ than other materials like steel or titanium, regarding not only the strength but also the fatigue life.

5. CONCLUSION AND FUTURE WORK

In this section, the results of the stress analysis and the fatigue life prediction using the FEA result will be summarized, and the future work required for the result that is more accurate will be suggested. This thesis proposed applying the pseudoelastic SMA to the TSJ because SMA has advantages compared to the steel and the titanium alloys as follows:

- The low elastic modulus of NiTi relative to steel and titanium results in a longer fatigue life for purely elastic deformation of the TSJ.
- The NiTi TSJ can reversibly undergo a large rotation that would cause the plastic yielding of steel and titanium TSJ.

5.1 Conclusions

Chapter 2 explained the stress analysis methods and fatigue life prediction methods focusing on the high cycle fatigue. First, the mathematical tool for modeling of TSJ system was introduced, and the reason why this thesis took that too for designing the TSJ was explained. The recommended design criteria to evaluate the designed TSJ model was also introduced. Second, the finite element method to analyze the pseudoelastic SMA TSJ system was introduced. Since this thesis decided to analyze the behavior of the pseudoelastic SMA TSJ with the steel and the titanium, the constitutive model of the linear elastic material was introduced for the FEM. Then, the 3D SMA constitutive model was introduced. Due to the material nonlinearity, SMA requires the subroutine using the return mapping algorithm to be analyzed via the finite element

method. In this thesis, the selected FEA program is Abaqus/Standard, and the subroutine is the Fortran coded UMAT. How the FE method solves the nonlinear equations generated by the return mapping algorithm, and the subroutine was briefly explained. Finally, the methods for the fatigue life prediction via stress-life curves were reviewed.

Chapter 3 explained the finite element model of pseudoelastic SMA TSJ system. First, the model geometry based on the optimization implemented by Gordon was introduced. By using the FEA program, Abaqus generated FE model was validated by comparison to the results of Gordon. The properties of the materials were also specified with the strength and the fatigue data. To the next, the top tension that is applied to the top of the TSJ was discussed and determined considering the effective tension over the top tensioned riser. For the application of the NiTi to the FE TSJ model, the transformation temperatures of the NiTi was selected considering the operating temperature and the applied top tension.

Chapter 4 analyzed the data obtained from the FEA to implement the stress analysis and the fatigue life prediction. First, the maximum stress distribution over the TSJ was analyzed to see that the pseudoelastic NiTi generates lower stress than the steel and the titanium at a given rotation due to the lower elastic modulus and the martensite transformation. The satisfaction of the design criteria was examined to see that the pseudoelastic NiTi TSJ survived at the 10-year hurricane, whereas the steel and the titanium TSJ did not. Then, the elastic behavior of the pseudoelastic NiTi TSJ before the martensite transformation initiates was analyzed regarding the yield angle and the maximum allowable angle of rotation at a given operating temperature. The

pseudoelastic behavior of the NiTi TSJ in one cyclic rotation was also analyzed. It was demonstrated that the martensite transformation reduced not only the maximum stress but also the stress amplitude, implying that the pseudoelastic effect is also beneficial regarding the fatigue life. Finally, the fatigue life of the pseudoelastic NiTi TSJ was predicted using the SWT and Morrow equation. Note that this fatigue life only considers the elastic deformation of the materials.

5.2 Future Work

In this thesis, it was concluded that the pseudoelastic SMA TSJ shows the better performance than currently used steel and titanium TSJ regarding the stress and the fatigue. This conclusion implies that the application of SMA to the component or the structure that are subjected to the cyclic stress can improve structural integrity and extend the service life. Still, several things should be researched in the future for the results that are more accurate, as follows.

- Model geometry: The model geometry of the TSJ used in this thesis is optimized only for the elastic material. Therefore, the optimization work should be done focusing on the SMA or NiTi alloy.
- Fatigue life prediction: In this thesis, the SWT and Morrow equations are used to estimate the fatigue life of the pseudoelastic NiTi TSJ. As discussed in the thesis, the SWT and Morrow equations consider the elastic strain only. Therefore, for predicting the fatigue life of the pseudoelastic NiTi TSJ including the martensite transformation, the fatigue data related to the plastic strain and the strain-life approach is required.

- Yield angle of the pseudoelastic NiTi TSJ: In this thesis, the yield angle of the NiTi TSJ was calculated by the constant *c* that assumes the elastic behavior only. However, the yield stress of the NiTi is reached after the martensite transformation. Therefore, the martensite transformation should be considered for calculating accurate yield angle of the NiTi TSJ.

REFERENCES

API. *API Standard 2RD: Dynamic Risers for Floating Production System.* 2nd ed. Washington, DC: American Petroleum Institute, 2009.

API. "Offshore Production Facilities." API.org. http://www.api.org/oil-and-natural-gas/wells-to-consumer/exploration-and-production/offshore/offshore-production-facilities (accessed June 10, 2017)

ASM International Handbook Committee. ASM Handbook, Volume 19: Fatigue and Fracture. ASM International, 1990.

Chang, S. H. M., Stanton, P., Kuriakose, S., & Thompson, H. "Sleeved stress joint for steel catenary riser application." *OMAE* (2010): 243-248.

Cheung, G. S. P. "A numerical method for predicting the bending fatigue life of NiTi and stainless steel root canal instruments." *International endodontic journal* 44(4) (2011): 357-361.

DNV. DNV-OS-F201: DYNAMIC RISERS. DET NORSKE VERITAS, 2010.

Dowling, N. "Mean Stress Effects in Stress-Life and Strain-Life Fatigue." *SAE* (2004)

Furlow, W. "Petronius faces delays." Offshore-mag.com. http://www.offshore-mag.com/articles/print/volume-58/issue-12/news/general-interest/petronius-faces-delays.html (accessed June 09, 2017)

Gordon, C. C., and Dareing, D. W. "Configuring Marine Riser Tapered Stress Joints Used in Top-Supported Applications." *Journal of Energy Resources Technology* 126(3) (2004): 201-207.

Kumar, P. K., and Lagoudas, D. C. “Introduction to Shape Memory Alloys.” In *Shape Memory Alloys: Modeling and Engineering Applications.* Springer US, 2008.

Lagoudas D. C., Bo Z., Qidwai M. A., and Entchev, P.B., “SMA UM: User Material Subroutine for Thermomechanical Constitutive Model of Shape Memory Alloys.” Smart Lab. http://smart.tamu.edu/SMAText/ (accessed June 13, 2017).

offshoretechllc. “Jacket Design.” offshoretechllc.com. http://www.offshoretechllc.com/fixed-platforms/ (accessed June 10, 2017)

offshore-technology. “Brutus, United States of America.” Offshore-technology.com. www.offshore-technology.com/projects/brutus/brutus4.html (accessed June 10, 2017)

Qidwai, M. A., Hartl, D. J., and Lagoudas, D. C. (2008). “Numerical implementation of an SMA thermomechanical constitutive model using return mapping algorithms.” In Shape Memory Alloys: Modeling and Engineering Applications. Springer US, 2008.

Reddy J. N. *An Introduction to the Finite Element Method,* 3rd ed. Boston: McGraw-Hill, 2004.

Rombado, G., Baker, D. A., Kan, W. C., Haldorsen, L. M., Craidy, P., and Hudak, S. J., Jr. “Fatigue Life Performance of Titanium Grade 29 Welds in Tapered Stress Joints.” *ISOPE* (2016): 606-611.

RTI Energy Systems, "Deepwater Engineering Solutions Using Titanium." RTI Energy Systems 2005. http://c.ymcdn.com/sites/www.titanium.org/resource/resmgr/2005_2009_papers/Boster_2005.pdf (accessed August 17, 2017).

Smart Lab, "Pseudoelastic Behavior." Smart Lab. http://smart.tamu.edu/overview/smaintro/simple/pseudoelastic.html (accessed June 9, 2017).

Sparks, C. P. *Fundamentals of Marine Riser Mechanics - Basic Principles and Simplified Analysis.* Tulsa: PennWell, 2007.

Tupper, E. C. and Rawson, K. *Basic Ship Theory, Combined Volume, Volume 2.* Oxford: Elsevier Science, 2001.

Vargas, P., Baxter, C., and Schutz, R. "A Level 3 BS7910 ECA for a Titanium Stress Joint for Use on a High Motion Floater in the Gulf of Mexico." *OMAE* 3 (2011): 81-591.

Yang, H., and Zheng, W. "Dynamic and Fatigue Analyses of Stress Joint for Deepwater Steel Catenary Riser." *OMAE* (2012): 65-70.

Zhang, Q., Zhang, R., Huang, Y., and Yang, H. "Design and Analysis of Taper Stress Joint for Top Tensioned Risers." *ISOPE* (2010): 23-28